Table 3
Correlations of the diffusion imaging parameters (Pearson's r) with the functional parameters

	Leg muscle contraction	Rota-rod treadmill	von Frey filament
FA	0.9851****	0.9451****	0.9667****
λ_1	0.9591****	0.9695****	0.9355****

**** $P<0.001$.

1 week, due to swelling of the degenerated myelin sheath, and decreased gradually thereafter, accompanied by the disappearance of myelin debris. Regenerating axons with a thin myelin sheath began to appear by 2–3 weeks after the injury. A few more small, regenerating axons with a myelin sheath thinner than that observed pre-injury were detected at 3–8 weeks, and their number approached the pre-injury level by 12 weeks, accompanied by maturation of the myelin sheaths (Fig. 4D).

Almost all the histological axonal parameters were correlated with the FA and λ_1 values at the distal site. The FA value, a parameter used to construct the DTT, was most strongly correlated with the axon density and axon diameter ($P<0.001$) (Table 2 and Fig. 5).

Functional recovery after peripheral nerve injury

We next investigated whether the changes in FA values and histological parameters were associated with functional recovery, using three different behavioral tests. To evaluate the recovery of motor function, we measured the degree of leg muscle contraction, and assessed the forelimb-hindlimb motor coordination using the Rota-rod treadmill test. Both of these tests showed the full recovery of motor function by 6 weeks after the injury ($P<0.05$) (Figs. 6A and B). Sensory function was evaluated using the von Frey filament test. Marked impairment was observed 1 day after the injury, after which the values gradually improved, returning to pre-injury levels by 6 weeks ($P<0.05$) (Fig. 6C). Thus, all three behavioral evaluations revealed functional recovery within 6 weeks in this experimental model.

The FA and λ_1 values at the lesion epicenter showed strong correlations with each of the aforementioned functional parameters ($P<0.001$) (Table 3 and Fig. 7).

Discussion

Methodological considerations

Beaulieu et al. reported that Wallerian degeneration after peripheral nerve injury reduces the anisotropy of water diffusion (Beaulieu et al., 1996; Stanisz et al., 2001). Their findings indicated that DTT might be useful for depicting the changes in anisotropy after peripheral nerve injury, and thus has tremendous potential as a tool for diagnosing peripheral nerve injury. However, although several preliminary studies for the DTT of peripheral nerves have been performed (Hiltunen et al., 2005; Meek et al., 2006; Skorpil et al., 2004), none has fully explored the potential of the DTI technology, especially its ability to depict the degeneration and regeneration of peripheral nerves after injury.

To apply DTT as a novel clinical tool for evaluating peripheral nerve injury, it is first necessary to acquire accurate data for visualizing Wallerian degeneration and regeneration. In the present study, we used a highly reproducible model, in which the rat sciatic nerve was subjected to contusive injury using an aneurysm clip, with a constant holding force. The histological changes in our model were similar to those in previously reported models of axonotmesis (Bridge et al., 1994; Varejao et al., 2004), in which spontaneous regeneration at a distal nerve section and functional recovery were also observed. We used 7.0-Tesla MRI to obtain the images, employing a conventional spin-echo protocol rather than echo planar imaging, to minimize distortion of the images due to phase errors accumulation during the data acquisition. To reduce motion artifacts, the MR images of excised nerves were obtained. Since previous studies have demonstrated degradation of the diffusion anisotropy in excised models (Madi et al., 2005; Matsuzawa et al., 1995), we captured all the images immediately after dissection of the sciatic nerve.

Interpretation of the diffusion anisotropy

The FA value at the lesion epicenter decreased immediately after the injury. On the other hand, at the distal site, while no significant change in the FA value was observed at 3 h or 1 day after the injury, a significant decrease in the value was observed 4 days after the injury. These results were consistent with the histological findings, which showed that the axons and myelin were preserved in the nerve segment distal to the lesion epicenter up to 1 day after the injury, with disintegration of the axonal structures and demyelination (Wallerian degeneration), being observed 4 days after the injury. The perineurium, the sheath of connective tissue that surrounds each neural fascicle, was still preserved (Lundborg, 2004; Sunderland, 1991) and regulated the diffusivity. As a result, while the axon density decreased to nearly zero (Fig. 4A) in the preserved fascicles, a less than 30% drop in the FA value was observed at 4 days after the injury. Thereafter, the FA value recovered gradually, reaching its pre-injury level by 3 weeks after the injury, when a few regenerating axons could be detected; that is, the FA value at the distal site returned to its pre-injury level prior to the histological recovery. Furthermore, the FA values at the lesion epicenter during recovery showed extremely strong correlations with each of the functional parameters examined.

To clarify the relevance of the changes in the FA values after peripheral nerve injury, we examined the correlations between the FA values and the quantitative changes in axonal properties. The FA values of the peripheral nerves were more strongly correlated with the axonal density and diameter than with the myelin density and thickness. These findings support the theories that the axonal

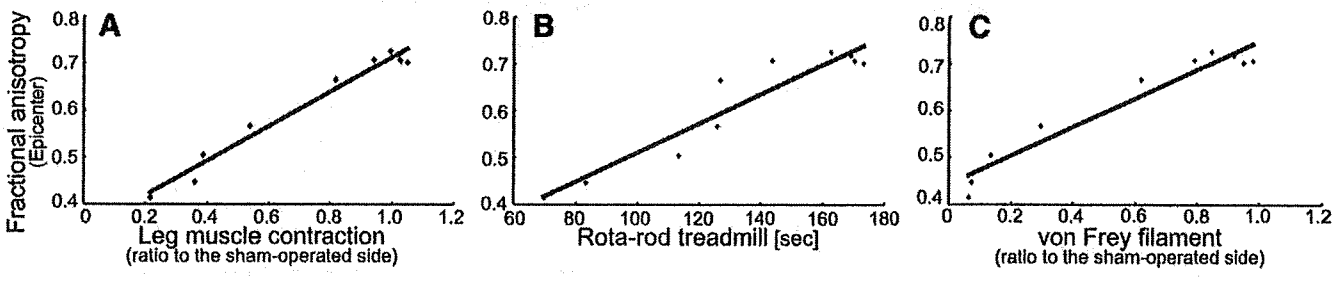

Fig. 7. Correlations between FA values and functional parameters. The FA values at the lesion epicenter were strongly correlated with each of the functional parameters (A, leg muscle contraction, $r=0.9851$, $P=0.000001$; B, Rota-rod treadmill, $r=0.9451$, $P=0.00004$; C, von Frey filament, $r=0.9667$, $P=0.000005$).

membranes play a major role in the anisotropic water diffusion in neural fibers (Beaulieu, 2002; Takahashi et al., 2002) and that myelination can modulate the degree of anisotropy (Gulani et al., 2001). The changes in the FA values after nerve injury mainly depended on λ_1, i.e., the axial diffusivity, consistent with the idea that water molecules preferentially diffuse along the longitudinal axis of axons, and degradation of the axonal cylinders would cause a loss of axial diffusivity. In addition, the absence of any significant change in the radial diffusivities (λ_2 and λ_3) might be explained by the present imaging conditions not being adequate to detect subtle changes of the radial diffusivities, which were significantly smaller than the axial diffusivity.

Potential clinical uses

Because it is difficult to distinguish peripheral nerves clearly from the surrounding tissues in conventional T1- and T2-weighted images, visualization of the Wallerian degeneration and regeneration of peripheral nerves after injury by MRI has been a challenge (Bendszus et al., 2002; Bendszus and Stoll, 2003; Bendszus et al., 2005; Filler et al., 1993; Howe et al., 1992; Kikuchi et al., 2003). In the present study, we were able to visualize these changes in peripheral nerves using DTI, and good correlations were found between the recovery as assessed by the changes in FA values and by histological and functional parameters. These findings support the applicability of DTI to the diagnosis of peripheral nerve injuries and monitoring of pathological conditions, to obtain information about the early phases of recovery in a clinical context.

We note that fiber tracking can sometimes terminate abruptly, because sharp bending or branching of the nerve can reduce the anisotropy below the tracking threshold (Hiltunen et al., 2005); therefore, the appropriate positioning and selection of a segment without branches will be critical, unless the spatial or angular resolution of the diffusion is greatly increased. In addition, although we have demonstrated the tracking and analysis of a straight sciatic nerve from the rat, which measures 1–1.5 mm in diameter and corresponds to the diameter of cutaneous nerves in humans, in voxels 0.31 mm in size, it is also important to keep in mind that the voxels forming the basis of the tracking are considerably larger than any individual axonal tract (Fujiyoshi et al., 2007).

We attempted to perform an in vivo study in a live model using smaller nerves to determine the feasibility of this method for clinical use (see Supplementary Materials), and we were able to demonstrate the recovery process of contused nerves in the same animal by tractography (Supplementary Fig. 3). Thus, DTT of the peripheral nerves could become an innovative tool for the evaluation of peripheral nerve injury, if applied correctly and with a clear understanding of its properties and limitations.

Acknowledgments

This work was supported by grants from the Leading Project for Realization of Regenerative Medicine from the Ministry of Education, Culture, Sports, Science and Technology (MEXT), Japan, from the Japan Science and Technology Corporation (JST), and from the General Insurance Association of Japan. This work was also supported by a Keio University grant-in-aid for encouragement of young medical scientists, by grants-in-aid for scientific research of MEXT, Japan, and by a grant-in-aid from the 21st Century COE Program of MEXT, Japan to Keio University. We thank Tokuko Harada and Hisako Takeuchi for tender animal care, Toshihiro Nagai for technical assistance with the electron microscope, and to all the other members of the spinal cord injury research team at Keio University School of Medicine for their enthusiastic discussions, encouragement, and invaluable comments on this study.

The authors declare no competing financial interests.

Appendix A. Supplementary data

Supplementary data associated with this article can be found, in the online version, at doi:10.1016/j.neuroimage.2008.09.022.

References

Basser, P.J., Mattiello, J., LeBihan, D., 1994. MR diffusion tensor spectroscopy and imaging. Biophys. J. 66, 259–267.
Beaulieu, C., 2002. The basis of anisotropic water diffusion in the nervous system — a technical review. NMR Biomed. 15, 435–455.
Beaulieu, C., Does, M.D., Snyder, R.E., Allen, P.S., 1996. Changes in water diffusion due to Wallerian degeneration in peripheral nerve. Magn. Reson. Med. 36, 627–631.
Bendszus, M., Stoll, G., 2003. Caught in the act: in vivo mapping of macrophage infiltration in nerve injury by magnetic resonance imaging. J. Neurosci. 23, 10892–10896.
Bendszus, M., Koltzenburg, M., Wessig, C., Solymosi, L., 2002. Sequential MR imaging of denervated muscle: experimental study. AJNR Am. J. Neuroradiol. 23, 1427–1431.
Bendszus, M., Wessig, C., Schutz, A., Horn, T., Kleinschnitz, C., Sommer, C., Misselwitz, B., Stoll, G., 2005. Assessment of nerve degeneration by gadofluorine M-enhanced magnetic resonance imaging. Ann. Neurol. 57, 388–395.
Bridge, P.M., Ball, D.J., Mackinnon, S.E., Nakao, Y., Brandt, K., Hunter, D.A., Hertl, C., 1994. Nerve crush injuries — a model for axonotmesis. Exp. Neurol. 127, 284–290.
Conturo, T.E., Lori, N.F., Cull, T.S., Akbudak, E., Snyder, A.Z., Shimony, J.S., McKinstry, R.C., Burton, H., Raichle, M.E., 1999. Tracking neuronal fiber pathways in the living human brain. Proc. Natl. Acad. Sci. U. S. A. 96, 10422–10427.
Filler, A.G., Howe, F.A., Hayes, C.E., Kliot, M., Winn, H.R., Bell, B.A., Griffiths, J.R., Tsuruda, J.S., 1993. Magnetic resonance neurography. Lancet 341, 659–661.
Filler, A.G., Maravilla, K.R., Tsuruda, J.S., 2004. MR neurography and muscle MR imaging for image diagnosis of disorders affecting the peripheral nerves and musculature. Neurol. Clin. 22, 643–682 vi-vii.
Fujiyoshi, K., Yamada, M., Nakamura, M., Yamane, J., Katoh, H., Kitamura, K., Kawai, K., Okada, S., Momoshima, S., Toyama, Y., Okano, H., 2007. In vivo tracing of neural tracts in the intact and injured spinal cord of marmosets by diffusion tensor tractography. J. Neurosci. 27, 11991–11998.
Gulani, V., Webb, A.G., Duncan, I.D., Lauterbur, P.C., 2001. Apparent diffusion tensor measurements in myelin-deficient rat spinal cords. Magn Reson Med 45, 191–195.
Hiltunen, J., Suortti, T., Arvela, S., Seppa, M., Joensuu, R., Hari, R., 2005. Diffusion tensor imaging and tractography of distal peripheral nerves at 3 T. Clin. Neurophysiol. 116, 2315–2323.
Howe, F.A., Filler, A.G., Bell, B.A., Griffiths, J.R., 1992. Magnetic resonance neurography. Magn. Reson. Med. 28, 328–338.
Kato, N., Nemoto, K., Nakanishi, K., Morishita, R., Kaneda, Y., Uenoyama, M., Ikeda, T., Fujikawa, K., 2005. Nonviral HVJ (hemagglutinating virus of Japan) liposome-mediated retrograde gene transfer of human hepatocyte growth factor into rat nervous system promotes functional and histological recovery of the crushed nerve. Neurosci. Res. 52, 299–310.
Kikuchi, Y., Nakamura, T., Takayama, S., Horiuchi, Y., Toyama, Y., 2003. MR imaging in the diagnosis of denervated and reinnervated skeletal muscles: experimental study in rats. Radiology 229, 861–867.
Lundborg, G., 2004. Nerve Injury and Repair, second ed. Elsevier, Philadelphia.
Mac Donald, C.L., Dikranian, K., Bayly, P., Holtzman, D., Brody, D., 2007a. Diffusion tensor imaging reliably detects experimental traumatic axonal injury and indicates approximate time of injury. J. Neurosci. 27, 11869–11876.
Mac Donald, C.L., Dikranian, K., Song, S.K., Bayly, P.V., Holtzman, D.M., Brody, D.L., 2007b. Detection of traumatic axonal injury with diffusion tensor imaging in a mouse model of traumatic brain injury. Exp. Neurol. 205, 116–131.
Madi, S., Hasan, K.M., Narayana, P.A., 2005. Diffusion tensor imaging of in vivo and excised rat spinal cord at 7 T with an icosahedral encoding scheme. Magn. Reson. Med. 53, 118–125.
Masutani, Y., Aoki, S., Abe, O., Hayashi, N., Otomo, K., 2003. MR diffusion tensor imaging: recent advance and new techniques for diffusion tensor visualization. Eur. J. Radiol. 46, 53–66.
Matsuzawa, H., Kwee, I.L., Nakada, T., 1995. Magnetic resonance axonography of the rat spinal cord: postmortem effects. J. Neurosurg. 83, 1023–1028.
Meek, M.F., Stenekes, M.W., Hoogduin, H.M., Nicolai, J.P., 2006. In vivo three-dimensional reconstruction of human median nerves by diffusion tensor imaging. Exp. Neurol. 198, 479–482.
Mori, S., Zhang, J., 2006. Principles of diffusion tensor imaging and its applications to basic neuroscience research. Neuron 51, 527–539.
Pierpaoli, C., Basser, P.J., 1996. Toward a quantitative assessment of diffusion anisotropy. Magn. Reson. Med. 36, 893–906.
Skorpil, M., Karlsson, M., Nordell, A., 2004. Peripheral nerve diffusion tensor imaging. Magn. Reson. Imaging 22, 743–745.
Song, S.K., Sun, S.W., Ju, W.K., Lin, S.J., Cross, A.H., Neufeld, A.H., 2003. Diffusion tensor imaging detects and differentiates axon and myelin degeneration in mouse optic nerve after retinal ischemia. Neuroimage 20, 1714–1722.
Stanisz, G.J., Midha, R., Munro, C.A., Henkelman, R.M., 2001. MR properties of rat sciatic nerve following trauma. Magn. Reson. Med. 45, 415–420.
Stejskal, E.O., Tanner, J.E., 1965. Spin diffusion measurements: spin echoes in the presence of a time dependent field gradient. J. Chem. Phys. 42, 288–292.
Sun, S.W., Liang, H.F., Cross, A.H., Song, S.K., 2008. Evolving Wallerian degeneration after transient retinal ischemia in mice characterized by diffusion tensor imaging. Neuroimage 40, 1–10.
Sunderland, S.S., 1991. Nerve Injuries and Their Repair: a Critical Appraisal. Churchill Livingstone, New York.
Takahashi, M., Hackney, D.B., Zhang, G., Wehrli, S.L., Wright, A.C., O'Brien, W.T., Uematsu, H., Wehrli, F.W., Selzer, M.E., 2002. Magnetic resonance microimaging of

intraaxonal water diffusion in live excised lamprey spinal cord. Proc. Natl. Acad. Sci. U. S. A. 99, 16192–16196.
Tamae, A., Nakatsuka, T., Koga, K., Kato, G., Furue, H., Katafuchi, T., Yoshimura, M., 2005. Direct inhibition of substantia gelatinosa neurones in the rat spinal cord by activation of dopamine D2-like receptors. J. Physiol. 568, 243–253.
Tuch, D.S., Wedeen, V.J., Dale, A.M., George, J.S., Belliveau, J.W., 2001. Conductivity tensor mapping of the human brain using diffusion tensor MRI. Proc. Natl. Acad. Sci. U. S. A. 98, 11697–11701.
Varejao, A.S., Cabrita, A.M., Meek, M.F., Bulas-Cruz, J., Melo-Pinto, P., Raimondo, S., Geuna, S., Giacobini-Robecchi, M.G., 2004. Functional and morphological assessment of a standardized rat sciatic nerve crush injury with a non-serrated clamp. J. Neurotrauma 21, 1652–1670.
Wessig, C., Jestaedt, L., Sereda, M.W., Bendszus, M., Stoll, G., 2008. Gadofluorine M-enhanced magnetic resonance nerve imaging: comparison between acute inflammatory and chronic degenerative demyelination in rats. Exp. Neurol. 210, 137–143.

Journal of Neuroscience Research 87:307–317 (2009)

Evaluation of Human Fetal Neural Stem/Progenitor Cells as a Source for Cell Replacement Therapy for Neurological Disorders: Properties and Tumorigenicity After Long-Term In Vitro Maintenance

Daisuke Ogawa,[1,2] Yohei Okada,[1,3] Masaya Nakamura,[4] Yonehiro Kanemura,[5] Hirotaka James Okano,[1] Yumi Matsuzaki,[1] Takuya Shimazaki,[1] Mamoru Ito,[6] Eiji Ikeda,[7] Takashi Tamiya,[2] Seigo Nagao,[2] and Hideyuki Okano[1]*

[1]Department of Physiology, School of Medicine, Keio University, Tokyo, Japan
[2]Department of Neurological Surgery, Faculty of Medicine, Kagawa University, Kagawa, Japan
[3]Department of Neurology, Graduate School of Medicine, Nagoya University, Nagoya, Japan
[4]Department of Orthopedic Surgery, School of Medicine, Keio University, Tokyo, Japan
[5]Institute for Clinical Research, Osaka National Hospital, National Hospital Organization, Osaka, Japan
[6]Central Institute for Experimental Animals, Tokyo, Japan
[7]Department of Pathology, School of Medicine, Keio University, Tokyo, Japan

It is expected that human neural stem/progenitor cells (hNS/PCs) will some day be used in cell replacement therapies. However, their availability is limited because of ethical issues, so they have to be expanded to obtain sufficient amounts for clinical application. Moreover, in-vitro-maintained hNS/PCs may have a potential for tumorigenicity that could be manifested after transplantation in vivo. In the present study, we demonstrate the in vitro and in vivo properties of long-term-expanded hNS/PCs, including a 6-month bioluminescence imaging (BLI) study of their in vivo tumorigenicity. hNS/PCs cultured for approximately 250 days in vitro (hNS/PCs-250) exhibited a higher growth rate and greater neurogenic potential than those cultured for approximately 500 days in vitro (hNS/PCs-500), which showed greater gliogenic potential. In vivo, both hNS/PCs-250 and -500 differentiated into neurons and astrocytes 4 weeks after being transplanted into the striatum of immunodeficient mice, and hNS/PCs-250 exhibited better survival than hNS/PCs-500 at this time point. We also found that the grafted hNS/PCs-250 survived stably and differentiated properly into neurons and astrocytes even 6 months after the surgery. Moreover, during the 6-month observation period by BLI, we did not detect any evidence of rapid tumorigenic growth of the grafted hNS/PCs, and neither PCNA/Ki67-positive proliferating cells nor significant malignant invasive features were detected histologically. These findings support the idea that hNS/PCs may represent a nontumorigenic, safe, and appropriate cell source for regenerative therapies for neurological disorders.

Key words: neural stem cell; in vivo optical imaging; long-term cultures; long-term engraftment; immunodeficient mouse

Recent progress in stem cell biology has greatly raised the expectation that cell replacement therapies may be developed for a variety of neurological disorders, such as spinal cord injury and neurodegenerative diseases, by using human fetal neural stem/progenitor cells (hNS/PCs) (Reynolds and Weiss, 1992; Svendsen et al., 1998; Carpenter et al., 1999; Uchida et al., 2000; Caldwell et al., 2001; Keyoung et al., 2001; Okano, 2002; Jeong et al., 2003; McBride et al., 2004; Cummings et al., 2005; Iwanami et al., 2005). However, the limited availability of human fetal tissues for ethical reasons makes it difficult to obtain large amounts of hNS/PCs. Therefore, for clinical applications, it is important to be able to expand hNS/PCs in vitro in a manner that maintains their multipotency and ability to self-renew.

Additional Supporting Information may be found in the online version of this article.

Contract grant sponsor: Leading Project for Realization of Regenerative Medicine from the Ministry of Education, Culture, Sports, Science and Technology (MEXT) of Japan; Contract grant sponsor: Japan Science and Technology Agency (SORST); Contract grant sponsor: Ministry of Health, Labor, and Welfare (to H.O.); Contract grant sponsor: Research Fellowships for Young Scientists from the Japan Society for the Promotion of Science (to Y.O.); Contract grant sponsor: Grant-in-Aid for 21st Century COE Program from the MEXT (to Keio University).

*Correspondence to: Hideyuki Okano, MD, PhD, Department of Physiology, Keio University School of Medicine, 35 Shinanomachi, Shinjuku-ku, Tokyo 160-8582, Japan. E-mail: hidokano@sc.itc.keio.ac.jp

Received 29 March 2008; Revised 12 June 2008; Accepted 13 June 2008

Published online 28 October 2008 in Wiley InterScience (www.interscience.wiley.com). DOI: 10.1002/jnr.21843

In addition, because of their low proliferation rate, it takes a long time for hNS/PCs to be expanded from a small number of cells to a sufficient population to use in cell replacement therapies. However, previous in vitro studies showed that subjecting hNS/PCs to multiple passages for up to 300 days in vitro (DIV) reduces their growth rate and alters their neurogenic potential (Caldwell et al., 2001; Kanemura et al., 2002; Piao et al., 2006; Wright et al., 2006; Anderson et al., 2007). Neither the proliferative and differentiation properties nor the in vivo dynamics have been reported for hNS/PCs cultured for longer than 300 DIV. Moreover, the long-term in vivo tumorigenicity of grafted hNS/PCs has never been described and is still uncertain.

Here we examined, both in vitro and in vivo, the differentiation and growth properties of hNS/PCs maintained for approximately 250 DIV (hNS/PCs-250) compared with hNS/PCs maintained for a longer period, approximately 500 DIV (hNS/PCs-500). Furthermore, we established a system for evaluating the in vivo tumorigenicity of hNS/PCs, by transplanting them into the striatum of immunodeficient mice and continuously monitoring the transplanted cells by bioluminescence imaging (BLI) in combination with conventional histology. With this system, we successfully monitored grafted cells for approximately 6 months, to evaluate the tumorigenicity of hNS/PCs as a source for cell replacement therapies.

MATERIALS AND METHODS

Cell Culture

Approval to use human fetal neural tissues and neurosphere cultures was obtained from the ethical committees of Keio University and Osaka National Hospital. Tissue procurement procedures were in accordance with the Declaration of Helsinki and in agreement with the ethical guidelines of the Japan Society of Obstetrics and Gynecology and with the ethical guidelines of the Network of European CNS Transplantation and Restoration (NECTAR). Forebrain tissues from a human fetus (8 weeks gestational age) were obtained from a legal abortion carried out at the Osaka National Hospital, with written informed consent obtained from the donor.

hNS/PCs were cultured using the neurosphere method (Reynolds and Weiss, 1992; Svendsen et al., 1998; Keyoung et al., 2001; Kanemura et al., 2002). The growth medium was a defined DMEM/F-12 (1:1)-based medium (Sigma, St. Louis, MO) supplemented with human recombinant (hr-) epidermal growth factor (20 ng/ml; PeproTech EC Inc., London, United Kingdom), hr-fibroblast growth factor 2 (20 ng/ml; PeproTech EC Inc.), hr-leukemia inhibitory factor (10 ng/ml; Chemicon, Temecula, CA), heparin (5 μg/ml; Sigma), B27 supplement (Invitrogen, Carlsbad, CA), and L-glutamine (200 mM; Invitrogen). Half of the culture medium was replaced with fresh growth medium every week. Neurospheres were passaged every 14 days by dissociating them into single cells using TrypLE select (Invitrogen). Viable cells (2×10^6 cells/15 ml) were seeded into 50% fresh growth medium plus 50% neurosphere-conditioned medium in uncoated T75 culture flasks and incubated at 37°C in 5% CO_2-95% air. hNS/PCs-250 represent neurospheres passaged 20–25 times; 244–314 DIV; mean 287.3 ± 24.2 DIV. hNS/PCs-500 represent neurospheres passaged 36–40 times; 476–526 DIV; mean 503.0 ± 18.8 DIV (mean ± SD).

To induce differentiation, the dissociated hNS/PCs were plated on poly-L-lysine (PLL)-coated coverslips and cultured in the DMEM/F-12/B27 without growth factors (Svendsen et al., 1998; Carpenter et al., 1999; Vescovi et al., 1999) for 7 days. On day 7, the cells were fixed in 4% paraformaldehyde (PFA) for 15 min and processed for immunocytochemical analysis.

Growth Assay

To measure the number of viable cells, the total ATP content was measured by ATP assay using the CellTiter-Glo Luminescent Cell Viability Assay (Promega, Madison, WI; Crouch et al., 1993; Petty et al., 1995). Single-cell suspensions were prepared from neurospheres by enzymatic dissociation with TrypLE select. The number of viable cells in the single-cell suspensions was determined by cell counting using trypan blue dye exclusion. To create a standard curve, 100-μl single-cell suspensions of known densities (1×10^5, 2×10^5, 4×10^5, and 8×10^5 cells/ml) were subjected to the ATP assay.

To assay the growth of hNS/PCs-250 and -500, single-cell suspensions from each neurosphere were plated in a 96-well plate (5×10^3 cells/100 μl). The cell number plated in each well on day 0 was equalized according to the ATP measurement, and the subsequent measurements were normalized to the value on day 0 (day 0 = 1, relative growth rate to day 0). Fresh medium (20 μl) was added every 4 days. The ATP assay was performed on days 0 (3 hr after plating), 2, 4, 7, and 11, by adding 100 μl of CellTiter-Glo Reagent to each well adjusted to 100 μl in advance. The luminescence signals were measured by a chemiluminescence detection system (Centro LB960; Berthold Technologies, Bad Wildbad, Germany).

Flow Cytometry

For cell-cycle analysis, the dissociated cells (1×10^6 cells) were incubated in 1 ml of hypotonic propidium iodide (PI) solution (1 mg/ml PI, 0.1% citric acid, 0.2% NP-40, 10 mg/ml RNaseA) (Deitch et al., 1982) for 30 min at 4°C, followed by a 15-min incubation at 37°C to digest the RNA. The fluorescent intensity of the PI was then measured by flow cytometry.

For the cell-surface marker analysis and viability assay, the dissociated cells were incubated in fresh medium at 37°C for 1 hr to recover the cell-surface antigens. The cells (1×10^7 cells) were suspended in 100 μl Hanks' balanced salt solution (HBSS) and incubated on ice for 30 min with allo phyco cyanin (APC)-conjugated anti-CD133 (Miltenyi Biotec, Tokyo, Japan) and phycoerythrin (PE)-conjugated anti-CD24 (BD Biosciences, Franklin Lakes, NJ), or fluorescvein isothiocyanate (FITC)-conjugated annexin V (BD Biosciences) to detect apoptosis. The cells were washed, resuspended in HBSS containing 1 μg/ml PI, and analyzed by FACS Caliber (BD Biosciences).

Virus Transduction and Bioluminescence Imaging

For the live monitoring of transplanted cells in vivo, we applied bioluminescent imaging (BLI), which has been described previously (Miyoshi et al., 1998; Okada et al., 2005). Human neurospheres and control U87MG cells were transduced by a lentivirus containing the click beetle red luciferase (CBR*luc*) coding sequence and Venus bicistronic reporter gene connected by an internal ribosomal entry site (IRES) (EF1α-CBRluc-IRES-Venus) (Supp. Info. Fig. 1A). The Venus-positive cells were then collected by a fluorescence-activated cell sorter (FACS) to establish cell lines that stably expressed Venus and CBR*luc*, as described previously (Masuda et al., 2007) (briefly summarized in Supp. Info. Fig. 1B). We confirmed that the photon counts from these CBR*luc*-labeled cells were directly proportional to the cell numbers plated in vitro (total cell numbers ranging from 10^2 to 10^6 cells/dish, Supp. Info. Fig. 1C,D). Moreover, the relative number of cells integrated into the host animals after transplantation could be estimated by measuring the photon counts from live animals after an intraperitoneal injection of D-luciferin. We also confirmed that the transduction with the lentivirus did not affect the proliferation or differentiation of hNS/PCs or the survival of the grafted animals (Supp. Info. Fig. 1E,F). A Xenogen-IVIS 100 cooled CCD optical macroscopic imaging system (Caliper Life Sciences, Hopkinton, MA) was used for BLI. All the images were analyzed with Igor (WaveMetrics, Lake Oswego, OR) and Living Image software (Caliper Life Sciences), and the optical signal intensity was expressed as photon counts, in units of photons per second. Each image was displayed as a pseudocolor photon count image superimposed on a gray-scale anatomic image. To quantify the measured luminescence, we defined a specific region of interest (ROI) that covered the area in and around the implanted cells. We used the same ROI for all the animals at all time points to ensure uniform data collection.

Transplantation

All the animal experiments were conducted according to the Guidelines for the Care and Use of Laboratory Animals of the Keio University School of Medicine. Mice were anesthetized and received implants of partially dissociated human neurospheres (2×10^6 cells in 4 μl of PBS) stereotactically into the right striatum (2 mm lateral and 1 mm anterior to bregma; depth 3 mm from dura). We used immunodeficient mice to avoid immunological rejection resulting from the xenograft. For short-term analyses of up to 4 weeks, we used *NOD/SCID/*γ_c^{null} (*NOG*) mice (Central Institute for Experimental Animals, Kanagawa, Japan), which are deficient for the common receptor gamma chain on the severe combined immunodeficiency (NOD/SCID) background (Ito et al., 2002) (n = 5 for hNS/PCs-250, n = 4 for hNS/PCs-500, n = 4 for U87MG). NOD/SCID mice (Charles River, Tokyo, Japan) were used for long-term observation of up to 6 months (n = 4 for hNS/PC-250, n = 4 for hNS/PCs-500, n = 4 for U87MG).

Animals were anesthetized and transcardially perfused with 4% PFA at 4 weeks (1 month), 12 weeks (3 months), and 24 weeks (6 months) after transplantation. The whole brain was removed and postfixed for 8 hr in 4% paraformaldehyde (PFA), soaked overnight in 15% followed by 30% sucrose, and embedded in OCT compound. Coronal sections 14 μm thick were made with a Cryostat (Leica, Wetzlar, Germany) and processed for immunohistochemical analysis.

Immunohistochemistry and Immunocytochemistry

For immunofluorescence analyses, cultured cells or tissue sections were incubated with the following primary antibodies at 4°C overnight: anti-human Nestin (1:30,000, rabbit polyclonal) (Nakamura et al., 2003), anti-TuJ-1 (1:500, mouse IgG2b monoclonal) (Sigma), antiglial fiibrillary acidic protein (GFAP) (1:3,000, rabbit polyclonal, Sigma), anti-green fluorescent protein (GFP; 1:25,000, mouse IgG2a, mFX72; a gift from Dr. S. Mitani), anti-Ki67 (1:500, Rb polyclonal IgG) (Novocastra Laboratories, Newcastle Upon Tyne, United Kingdom), antiproliferating cell nuclear antigen (PCNA) (1:1,000; Rb polyclonal IgG) (Oncogene, Boston MA), and anti-human nuclei (1:100, mouse monoclonal IgG1) (Chemicon). After three washes, the samples were incubated with Alexa 488-, 555-, or 647-conjugated secondary antibodies (Invitrogen) for 2 hr at room temperature. Images were obtained by microscopy (Apotome; Carl Zeiss) or confocal laser scanning microscopy (LSM510; Carl Zeiss).

The quantification of different phenotypes in vitro was accomplished by counting the immunolabeled cells on each coverslip. Five separate, randomly chosen fields on each coverslip were counted using a ×20 objective. The numbers of Nestin-, TuJ-1-, and GFAP-immunoreactive cells are presented as the percentage of total cells, which were stained by Hoechst 33258.

To quantify the Ki67-, PCNA-, and TUNEL-positive cells in tissue sections, the number of immunoreactive cells that were also positively stained by anti-human nuclei were counted in more than five randomly selected fields in each section. These data are presented as the percentage of total cells stained by human antinuclear antigen. Hematoxylin-eosin (HE) staining and HRP-DAB staining were carried out according to standard histological protocols.

Statistical Analysis

Statistical analyses were performed with Student's *t*-test and Dunn's test. Values are presented as the mean ± SEM. Significance was accepted at $P < 0.05$.

RESULTS

hNS/PCs Cultured for Long Periods Lost Their Proliferation Ability In Vitro

We first compared the properties of hNS/PCs-250 with those of hNS/PCs-500 in vitro, including the growth rate and differentiation potentials. By ATP assay (Kanemura et al., 2002), hNS/PCs-250 exhibited a significantly higher growth rate than did hNS/PCs-500 (Fig. 1A). Cell-cycle analysis by PI staining showed that the proportion of dividing cells in S/G2/M was 20.5% ± 1.2% for hNS/PCs-250, which was significantly higher than that for hNS/PCs-500 (12.7% ± 0.2%) (n = 3, $P < 0.01$; Fig. 1B). However, there was no

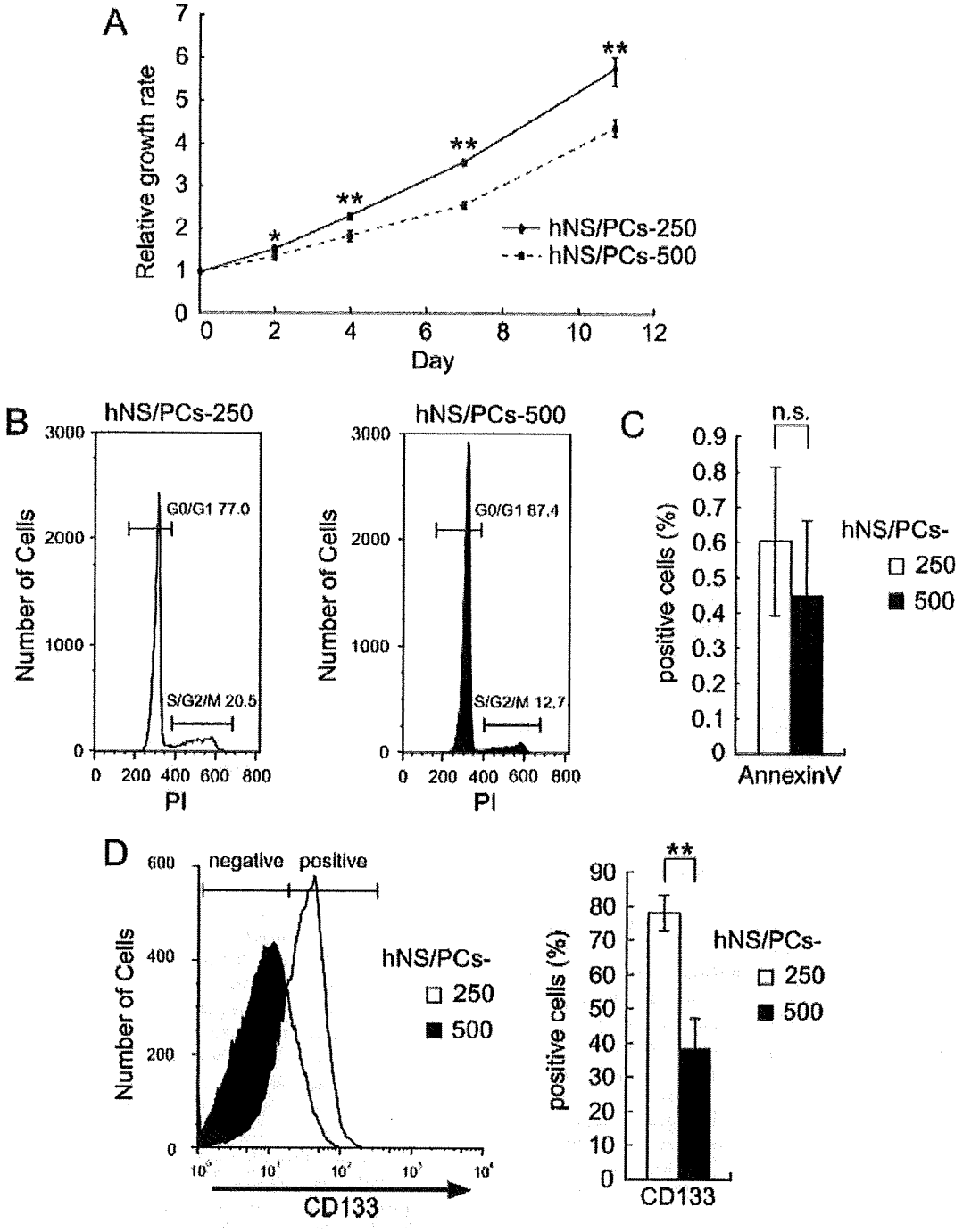

Fig. 1. Comparison of the in vitro properties of hNS/PCs-250 and -500. **A:** Growth rate of hNS/PCs-250 and -500 examined by ATP assay. hNS/PCs-250 exhibited a significantly higher growth rate than did hNS/PCs-500 during 11 days of culture. **B:** Cell-cycle analysis by PI staining. The proportion of dividing cells in S/G2/M was significantly higher in hNS/PCs-250 than in -500 ($P < 0.01$). **C:** Analysis of apoptotic cells by annexin V staining. No significant difference in the proportions of annexin V-positive cells was observed between hNS/PCs-250 and -500. n.s., Not significant ($P > 0.05$). **D:** Expression of CD133, a marker for undifferentiated hNS/PCs, in hNS/PCs-250 and -500 analyzed by flow cytometry. hNS/PCs-250 contained significantly more $CD133^+$ cells than did -500. All data are presented as the mean ± SEM (n = 3). $*P < 0.05$; $**P < 0.01$.

significant difference in the proportion of apoptotic cells stained with annexin V between hNS/PCs-250 and -500 (Fig. 1C). These results suggest that the difference in the in vitro growth rate between hNS/PCs-250 and -500 by ATP assay might be attributable to the presence of a differing proportion of proliferating cells, but not of apoptotic cells.

We speculated, based on these results, that there might be a difference in the proportion of undifferentiated hNS/PCs in the neurospheres of hNS/PCs-250 and -500. Therefore, we examined dissociated neurospheres for the expression of cell-type-specific surface markers by flow cytometry. The results indicated that the proportion of $CD133^+$ cells, which are known to represent an enriched population of neurosphere-initiating cells (Uchida et al., 2000; Barraud et al., 2007; Panchision et al., 2007), in hNS/PCs-250 was approximately twice that in hNS/PCs-500 (77.9% ± 5.2% and 38.2% ± 8.9% in hNS/PCs-250 and -500, respectively, $P < 0.01$; Fig. 1D), suggesting that the $CD133^+$ hNS/PCs in neurospheres may contribute to the higher growth rate seen in hNS/PCs-250 vs. hNS/PCs-500.

hNS/PCs-250 Generated Relatively More Neurons, Whereas hNS/PCs-500 Generated More Astrocytes

We next allowed hNS/PCs-250 and -500 to differentiate on PLL-coated coverglasses without growth factors for 7 days and examined their phenotypes by immunocytochemistry. There was no significant difference in the percentage of Nestin-positive cells between hNS/PCs-250 and -500 (Fig. 2A,B). However, whereas more than 50% of the hNS/PCs-250 differentiated into TuJ-1-positive neurons (54.3% ± 5.5% and 17.6% ± 3.0% in hNS/PCs-250 and -500, respectively, n = 3, $P < 0.01$), more than 70% of the hNS/PCs-500 differentiated into GFAP-positive astrocytes (23.6% ± 14.7% and 73.5% ± 6.6% in hNS/PCs-250 and -500, respectively, n = 3, $P < 0.05$). As previously reported, neither hNS/PCs-250 nor hNS/PCs-500 differentiated into CNPase-positive oligodendrocytes in vitro under the same conditions (Iwanami et al., 2005) (data not shown). Consistently with these findings, flow cytometric analyses showed that hNS/PCs-250 contained a greater proportion of $CD24^+$ cells, which are proposed to include the cells committed to neuronal lineages (Calaora et al., 1996; Shewan et al., 1996; Doetsch et al., 1999; Nieoullon et al., 2005; Panchision et al., 2007), than did hNS/PCs-500 (73.2% ± 5.4% and 56.1% ± 5.4% in hNS/PCs-250 and -500, respectively, n = 3, $P < 0.05$; Fig. 2C). Interestingly, most and some of the $CD24^+$ cells in the hNS/PCs-250 and -500 were also positive for CD133 (82.2% and 41.8%, respectively; Fig. 2D). Therefore, we also analyzed the $CD133^-$ populations and found that the proportion of $CD133^-$ cells that were $CD24^+$, possibly those representing neuronal progenitors and postmitotic neurons, tended to be higher in the hNS/PCs-250 than in the hNS/PCs-500, although the difference was not statistically significant (61.1% and 51.6% in hNS/PCs-250 and -500, respectively, $P = 0.06$; Fig. 2D). Taken together, these findings suggest that hNS/PCs-250 may contain more neurogenic progenitors than do the hNS/PCs-500, which contain more gliogenic progenitors.

hNS/PCs-250 Exhibited Better Survival After Transplantation Into the Striatum of NOG Mice Than Did hNS/PCs-500 by In Vivo Imaging

To assess the survival and differentiation potentials of hNS/PCs in vivo, we stereotactically transplanted hNS/PCs-250, hNS/PCs-500, or U87MG cells, a human glioblastoma cell line, into the right striatum of the intact mouse brain. To avoid immunological rejection of the grafted cells, we used NOG mice (Ito et al., 2002), which are deficient for the interleukin-2 receptor common γ chains under the background of severe combined immunodeficiency (NOD/SCID) mice (Shultz et al., 1995).

After transplantation, we observed the survival and growth of the grafted hNS/PCs and U87MG cells for up to 4 weeks (n = 4 each). For the live monitoring of transplanted cells in vivo, we labeled the hNS/PCs and U87MG with a lentivirus containing the coding sequence for CBR*luc* and a Venus reporter gene (EF1α-CBR*luc*-IRES-Venus) (Supp. Info. Fig. 1A) and applied BLI (Okada et al., 2005). The BLI results revealed that the surviving grafted hNS/PCs-250 and -500 decreased sharply, to approximately 20–40% of their original levels 1 week after the transplantation and were maintained thereafter. Four weeks after the transplantation, hNS/PCs-250 showed significantly better survival than did hNS/PCs-500 (12.7% ± 2.4% and 3.8% ± 1.0% of the initial photon counts in hNS/PCs-250 and -500, respectively, n = 4, $P < 0.01$; Fig. 3A,B). In contrast, the U87MG glioblastoma cells showed logarithmic growth during the 4-week observation period.

Immunohistochemical analyses revealed that both hNS/PCs-250 and hNS/PCs-500 had differentiated into TuJ1-positive neurons and GFAP-positive astrocytes 4 weeks after the transplantation (Fig. 4A). Nestin-positive neural progenitors were also observed in both the hNS/PCs-250 and the hNS/PCs-500 grafts. hNS/PCs-250 contained significantly more Ki67- and PCNA-positive cells than did hNS/PCs-500 (Ki67: 5.1% ± 0.8% and 3.1% ± 0.3%, $P < 0.05$; PCNA: 5.8% ± 0.2% and 4.4% ± 0.3%, in hNS/PCs-250 and -500, respectively, n = 3, $P < 0.01$; Fig. 4B,C). The percentage of TUNEL-positive apoptotic cells was not significantly different between hNS/PCs-250 and hNS/PCs-500 (0.26% ± 0.05% and 0.37% ± 0.14%, respectively, n = 3; Fig. 4D,E).

Grafted Neurospheres Survived and Differentiated Into Neurons and Astrocytes In Vivo but Did Not Show Tumorigenicity Even 6 Months After Transplantation

Finally, we evaluated the long-term survival of hNS/PCs and investigated their safety as a cell source

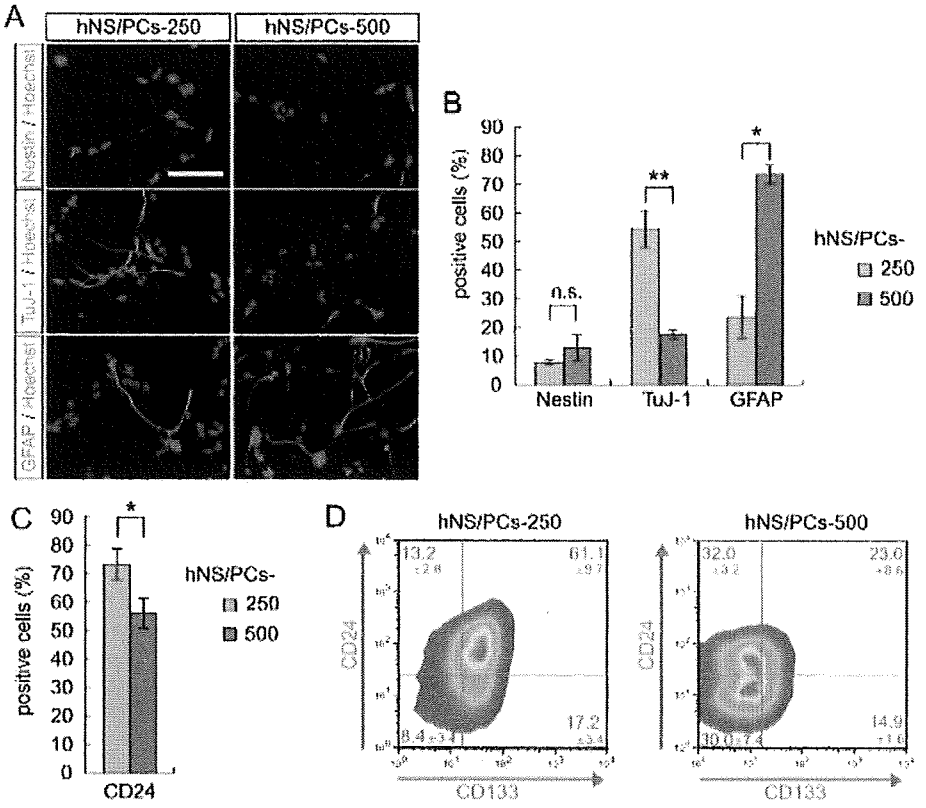

Fig. 2. Altered differentiation potentials between hNS/PCs-250 and -500. **A:** Immunocytochemical analysis of differentiated hNS/PCs for markers of neural progenitors (Nestin), neurons (TuJ-1), and astrocytes (GFAP). Quantitative analysis is shown in **B**. Only approximately 10% of the cells in both hNS/PCs-250 and -500 remained positive for Nestin. hNS/PCs-250 differentiated into significantly more TuJ-1-positive neurons than did hNS/PCs-500, whereas hNS/PCs-500 differentiated into significantly more GFAP-positive astrocytes than did hNS/PCs-250. **C:** Flow cytometric analysis of CD24, which is expressed in populations that include neuronal progenitors and postmitotic neurons. Consistent with the results in B, hNS/PCs-250 contained significantly more CD24-positive cells than did hNS/PCs-500. **D:** Coexpression of CD133 and CD24 by flow cytometric analysis. Consistently with the results in Figures 1 and 2B, hNS/PCs-250 contained significantly more $CD133^+$ cells and $CD24^+$ cells than did hNS/PCs-500; n = 3; means ± SEM. $*P < 0.05$; $**P < 0.01$; n.s., not significant ($P > 0.05$). Scale bar = 50 μm.

for transplantation therapy. For long-term observation, we used NOD/SCID mice, which are resistant to stress and infection and therefore show better survival than NOG mice. The results of the short-term experiment revealed that hNS/PCs-500 showed a lower proliferation ability than hNS/PCs-250 in vivo by Ki67 or PCNA immunostaining and a poor survival rate by BLI (only 3.8% 1 month after transplantation even in NOG mice) (Fig. 3A). Thus, for this long-term experiment, we monitored the in vivo tumorigenicity of only the hNS/PCs-250, as the better cell source for cell replacement therapy.

We transplanted hNS/PCs-250 into the right striatum of NOD/SCID mice and observed the survival of the grafted hNS/PCs by BLI for 6 months. The photon count of the luminescence generated by the surviving hNS/PCs was reduced to 12.8% ± 11.0% of the initial photon count at 8 weeks and thereafter maintained its signal for 6 months (10.0% ± 14.0%, n = 4; Fig. 5A). Notably, no rapid tumorigenic increase of the grafted hNS/PCs was observed within the 6 months following the transplantation. In contrast, control U87MG cells grew rapidly, showing a 419% increase in photon count 4 weeks after transplantation. Among the U87MG-transplanted mice, 75% (three of four) died by 5 weeks and the rest by 6 weeks after transplantation.

To examine the phenotype of the surviving cells derived from the transplanted hNS/PCs, we performed immunohistochemical analyses. Consistent with the findings of BLI, surviving Venus-positive cells were detected 3 months after transplantation (Fig. 5B). Most of them resided at the transplantation site for the entire 6 months and differentiated into TuJ-1-positive neurons and GFAP-positive astrocytes (Fig. 5C). In addition, Nestin-positive neural progenitors persisted even 6 months after the transplantation. However, the grafted hNS/PCs 6 months after transplantation in the long-term animals appeared to have larger nuclei and

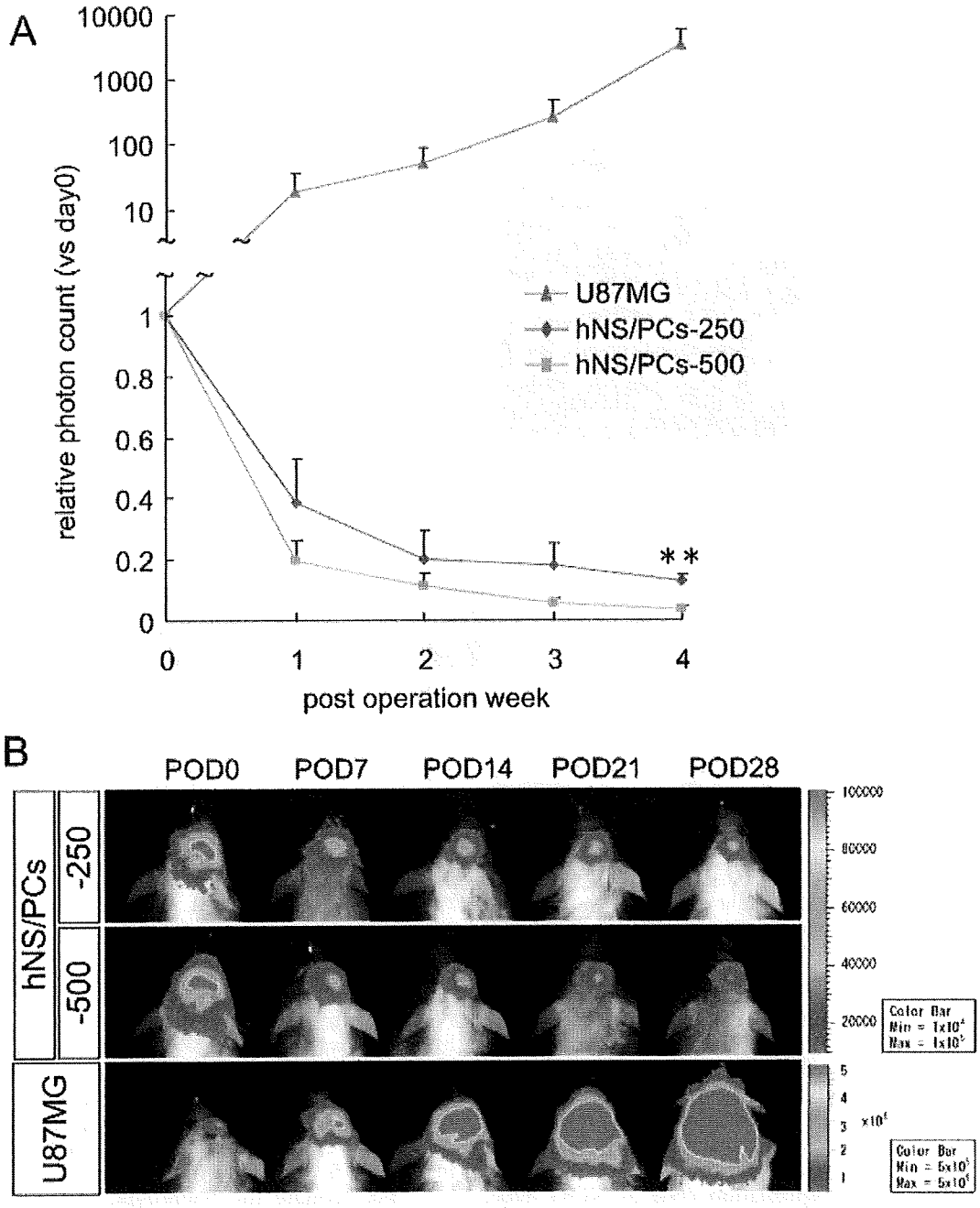

Fig. 3. Bioluminescence imaging of hNS/PCs-250 and -500 transplanted into NOG mice for up to 4 weeks. **A:** hNS/PCs-250, -500, and human glioblastoma cells (U87MG) were transplanted into the right striatum of NOG mice and observed by BLI for up to 4 weeks. hNS/PCs-250 exhibited significantly better survival and growth than did hNS/PCs-500 4 weeks after transplantation (n = 4; means ± SEM). $^{**}P < 0.01$. **B:** Representative BLI images of the treated mice.

lower cell densities than those observed 4 weeks after transplantation in the short-term animals (Fig. 5D). Importantly, we did not find any proliferating cells labeled by Ki67 or PCNA 6 months after transplantation (Fig. 5E) nor any obvious evidence of malignant invasive behavior by HE staining (Fig. 5F). Together

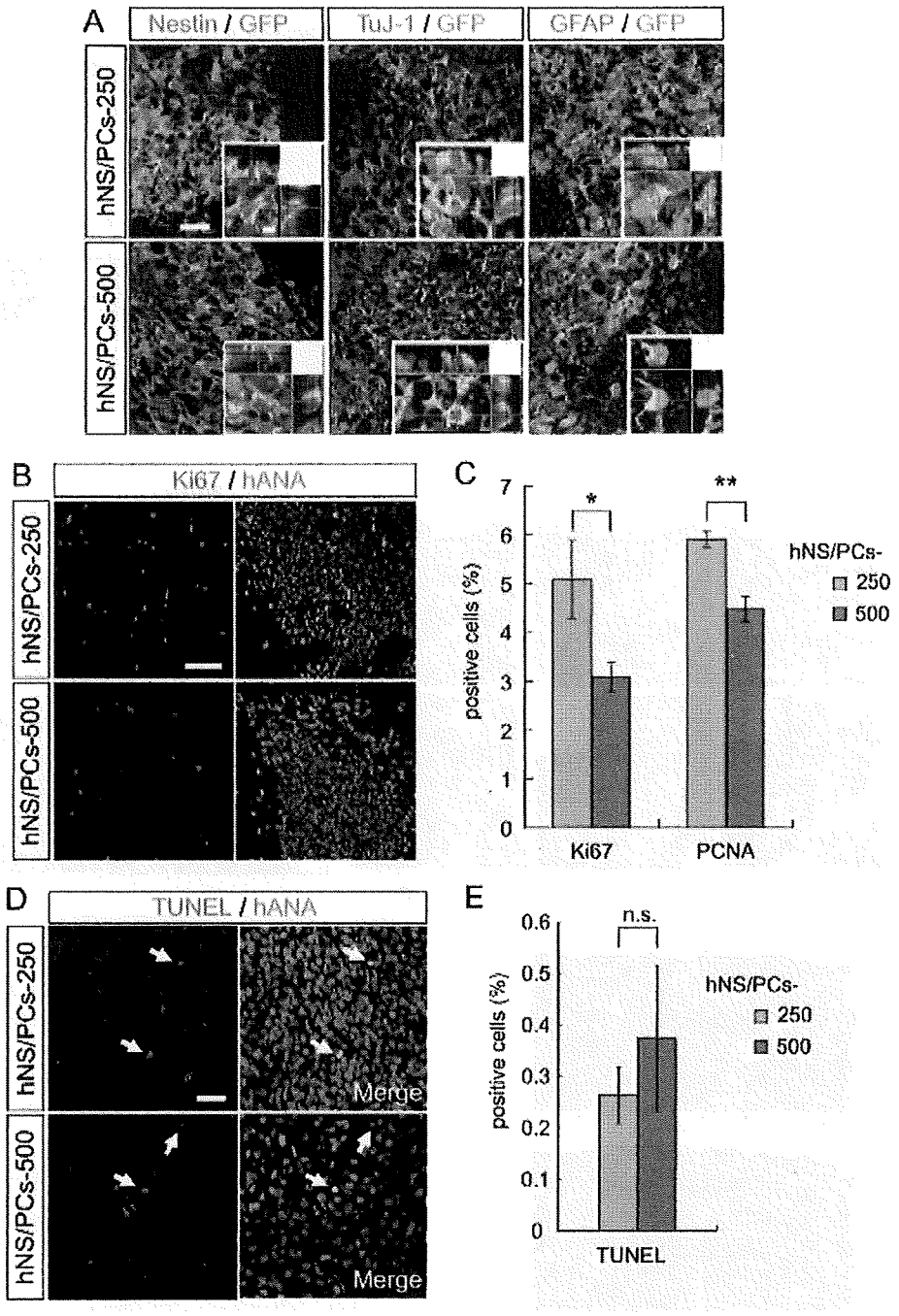

Fig. 4. Both hNS/PCs-250 and -500 appropriately differentiated into neurons and astrocytes in vivo. **A:** Immunofluorescence analysis of tissue sections 4 weeks after transplantation. Although some of the grafted hNS/PCs-250 and -500 still expressed Nestin, they had also differentiated into TuJ-1-positive neurons and GFAP-positive astrocytes. **B:** Representative image of Ki67-positive proliferating cells in the hNS/PCs-250 and -500 grafts. **C:** Quantitative analysis of the proportion of Ki67- and PCNA-positive cells in grafted hNS/PCs-250 and -500 4 weeks after transplantation. hNS/PCs-250 showed a significantly higher proportion of proliferating cells than did hNS/PCs-500. **D:** Analysis of apoptotic cells by TUNEL staining in grafted hNS/PCs. **E:** Quantitative analysis of TUNEL-positive cells. No significant difference in the TUNEL-positive apoptotic cells was observed between hNS/PCs-250 and -500. All data are presented as the mean ± SEM; n = 3. $*P < 0.05$; $**P < 0.01$; n.s., not significant. Scale bars = 20 μm and 5 μm for low- and high-magnification images, respectively, in A; 50 μm in B; 20 μm in D.

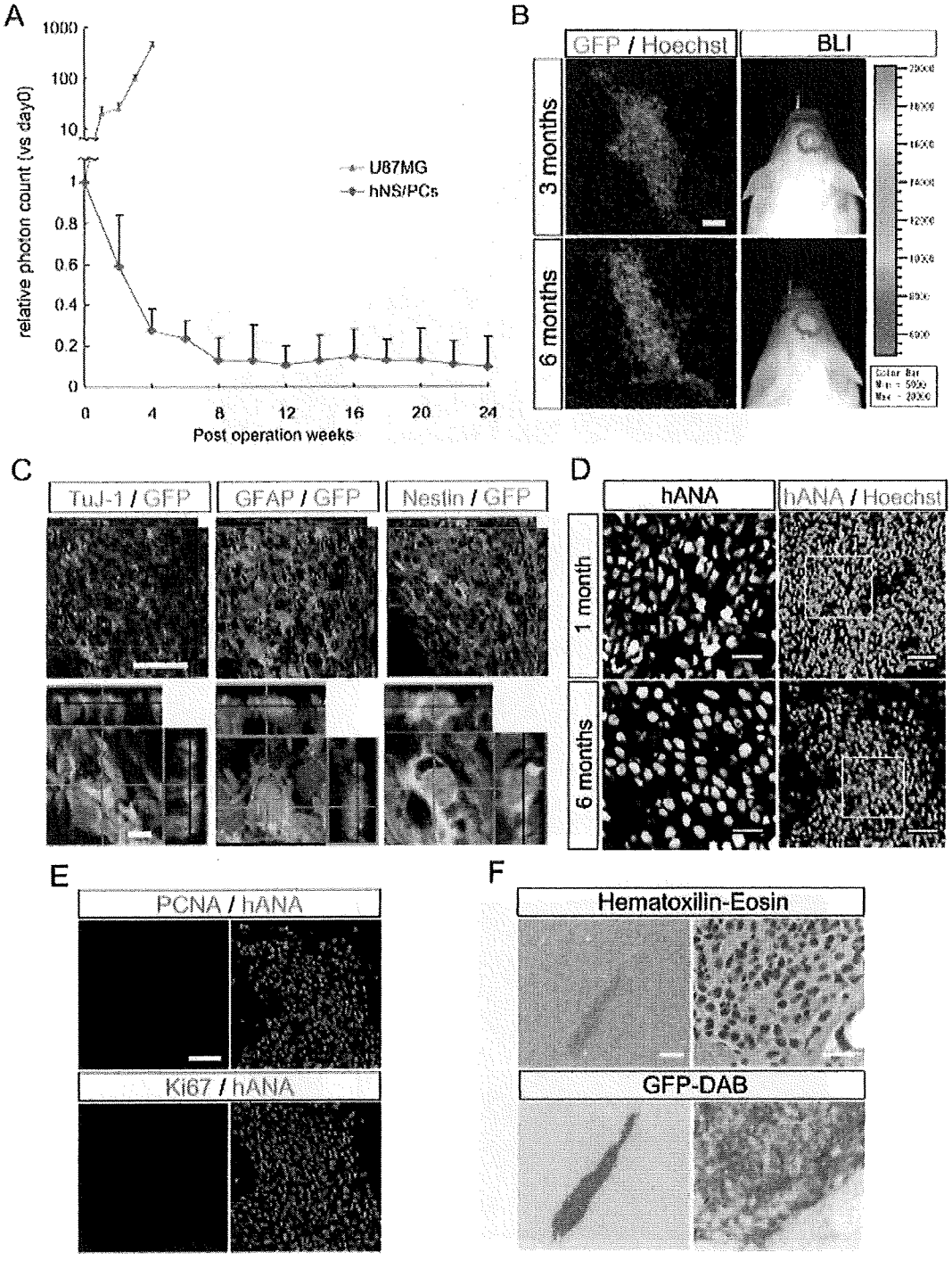

Fig. 5. hNS/PCs did not exhibit tumorigenesis for 6 months. **A:** Long-term observation of grafted hNS/PCs-250 by BLI for 6 months. The photon count of hNS/PCs decreased for 8 weeks after transplantation but was stable thereafter. The hNS/PCs did not show any evidence of tumorigenicity during the 6-month observation period, unlike the control U87MG cells. Data are presented as the mean ± SEM. **B:** Immunohistochemical analysis of Venus-expressing grafted hNS/PCs 3 and 6 months after transplantation showed consistent correlation of the Venus-expressing area with the photon counts detected by BLI. **C:** Immunohistochemical analysis of grafted hNS/PCs 6 months after transplantation. hNS/PCs resided at the site of injection and differentiated into TuJ-1-positive neurons and GFAP-positive astrocytes. However, Nestin-positive neural progenitors were also observed, even 6 months after transplantation. **D:** hANA and Hoechst nuclear staining of the grafted area 1 month and 6 months after the transplantation. Grafted cells showed larger nuclei and lower cell densities in the long-term analysis than in the short-term analysis. **E:** Immunohistochemical analysis of proliferation markers PCNA and Ki67. Neither PCNA- nor Ki67-positive cells were observed. **F:** Hematoxylin-eosin and GFP-DAB staining indicated no malignant invasive features in the transplanted cells. Scale bars = 100 μm in B; low-magnification image 50 μm, high-magnification image 5 μm in C; low-magnification image 50 μm, high-magnification image 20 μm in D; 50 μm in E; low-magnification image 200 μm, high-magnification image 20 μm in F.

these findings indicate that the grafted hNS/PCs could survive and differentiate properly in the brain of NOD/SCID mice without any tumor formation, at least for 6 months after transplantation.

DISCUSSION

Human Fetal Neurospheres Exhibited Altered Proliferation and Differentiation Properties In Vitro and In Vivo, Depending on the Culture Period

Because large numbers of human fetus-derived cells are difficult to obtain unless they are expanded in vitro, it is essential to evaluate the differentiation and proliferation properties as well as tumorigenic potential of in-vitro-expanded hNS/PCs when considering their clinical use in cell replacement therapies. In the present study, we clearly showed the likely senescence of hNS/PCs maintained for more than 500 DIV, from their differentiation and proliferation properties. More importantly, we also showed the lack of tumorigenicity of hNS/PCs-250 over the long term in vivo. This is the first report in which the in vivo tumorigenicity of transplanted in-vitro-maintained hNS/PCs was evaluated by long-term monitoring with BLI.

The in vitro ATP assay (Fig. 1A) and in vivo BLI study (Fig. 3A) showed that hNS/PCs-250 had significantly higher growth and survival rates than did hNS/PCs-500 both in vitro and in vivo. This difference between hNS/PCs-250 and -500 in vitro was attributable to a reduced proportion of dividing cells in the hNS/PCs-500, shown by positive staining for Ki67 or PCNA, or in the cell cycle of S/G2/M, but not to the proportion of annexin V-positive apoptotic cells. In addition, the proportion of $CD133^+$ undifferentiated hNS/PCs was lower in the older hNS/PCs-500 than in the younger hNS/PCs-250. Thus, hNS/PCs seem to lose their ability to self-renew and acquire the properties of committed progenitors or postmitotic cells during their long-term culture in vitro.

Interestingly, this difference in self-renewability between hNS/PCs-250 and -500 seemed to be correlated with an alteration in their differentiation potentials. hNS/PCs-250 exhibited more neurogenic and fewer gliogenic properties than hNS/PCs-500 (Fig. 2A,B). Given that the $CD24^+$ cells are proposed to be associated with the population of committed neuronal progenitors and neurons (Calaora et al., 1996; Shewan et al., 1996; Doetsch et al., 1999; Murayama et al., 2002; Nieoullon et al., 2005; Pruszak et al., 2007), the significantly higher proportion of $CD24^+$ cells in hNS/PCs-250 than in hNS/PCs-500 (Fig. 2C,D) also supports the idea that the hNS/PCs-250 contain more neurogenic progenitors than do the hNS/PCs-500, which contain more gliogenic progenitors. Taken together, these findings suggest that human fetal neurospheres lose multipotent and self-renewable hNS/PCs, which are replaced by progenitors committed to become glial cells, after long-term maintenance in vitro.

Long-Term Observation by BLI Revealed hNS/PCs To Be Nontumorigenic up to 6 Months After Their Transplantation Into NOD/SCID Striatum

Although some reports have examined the safety of grafted cells, including their long-term potential for tumorigenicity, by histological analyses, this type of analysis does not allow the dynamics of donor cells to be observed over time in the same live animal. In the present study, we monitored the survival of hNS/PCs grafted into the NOD/SCID striatum by BLI. Because we do not have to sacrifice the animals at each time point for histological analysis, we can repeatedly examine the same grafted animal and sequentially evaluate the in vivo tumorigenicity of the donor cells. This monitoring system allows a more accurate analysis than the conventional intermittent histological method.

The findings that the photon counts of engrafted hNS/PCs-250 decreased to 12.8% of the initial count within 8 weeks after transplantation and that their signals were maintained thereafter for up to 6 months without any tumorigenic proliferation, unlike the U87MG glioblastoma cell line, suggested that hNS/PCs-250 are not tumorigenic. These results were confirmed by histological analyses. The Venus-positive area 6 months after transplantation was no greater than the area 3 months after the surgery. No Ki67- or PCNA-positive proliferative cells were observed 6 months after the transplantation. HE staining indicated a pathology that lacked any malignant invasive behavior. Taken together, these results strongly indicate that the hNS/PCs-250 were negative for tumorigenicity. Surprisingly, the Venus-positive grafted cells were still positive for Nestin even 6 months after the transplantation, but they were negative for the proliferation markers Ki67 and PCNA (Fig. 5E). Moreover, the density of the grafted cells was much lower in animals 6 months after grafting than 1 month after grafting (Fig. 5D). Although we cannot clarify the properties of these Nestin-positive but proliferation marker-negative cells, they might reside in the grafted sites as dormant neural stem cells. Therefore, further evaluation of the safety of these donor cells, such as observation periods much longer than 6 months, is warranted.

In conclusion, we showed that the maintenance and safety of transplanted hNS/PCs could be assessed by monitoring the dynamics of these cells in vivo using BLI. Our present study provides a reliable system for evaluating the tumorigenicity of hNS/PCs in vivo and addresses several issues that are prerequisites for the clinical application of hNS/PCs, including defining their properties in vitro and in vivo and their tumorigenicity when transplanted after long-term maintenance in culture. Taken together with previous reports, our data indicate that the prospect for the future application of hNS/PCs to cell replacement therapies for neurological disorders is very promising.

ACKNOWLEDGMENTS

We are grateful to Dr. S. Mitani for the anti-GFP antibody; Drs. T. Nomura and K. Tamaoki for the NOG mice; Dr. M. Yamasaki for the human neural

stem/progenitor cells; Dr. H. Miyoshi for the lenti-virus vector; Dr. Y. Toyama for continuous encouragement; Mrs. Y. Yamashita, Ms. A. Yokokawa, and Mrs. T. Harada for technical assistance; and all the members of Dr. Okano's laboratory for encouragement and kind support.

REFERENCES

Anderson L, Burnstein RM, He X, Luce R, Furlong R, Foltynie T, Sykacek P, Menon DK, Caldwell MA. 2007. Gene expression changes in long term expanded human neural progenitor cells passaged by chopping lead to loss of neurogenic potential in vivo. Exp Neurol 204:512–524.

Barraud P, Stott S, Mollgard K, Parmar M, Anders B. 2007. In vitro characterization of a human neural progenitor cell coexpressing SSEA4 and CD133. J Neurosci Res 85:250–259.

Calaora V, Chazal G, Nielsen PJ, Rougon G, Moreau H. 1996. mCD24 expression in the developing mouse brain and in zones of secondary neurogenesis in the adult. Neuroscience 73:581–594.

Caldwell MA, He X, Wilkie N, Pollack S, Marshall G, Wafford KA, Svendsen CN. 2001. Growth factors regulate the survival and fate of cells derived from human neurospheres. Nat Biotechnol 19:475–479.

Carpenter MK, Cui X, Hu Z, Jackson J, Sherman S, Seiger A, Wahlberg LU. 1999. In vitro expansion of a multipotent population of human neural progenitor cells. Exp Neurol 158:265–278.

Crouch SPM, Kozlowski R, Slater KJ, Fletcher J. 1993. The use of ATP bioluminescence as a measure of cell proliferation and cytotoxicity. J Immunol Methods 160:81–88.

Cummings BJ, Uchida N, Tamaki SJ, Salazar DL, Hooshmand M, Summers R, Gage FH, Anderson AJ. 2005. Human neural stem cells differentiate and promote locomotor recovery in spinal cord-injured mice. Proc Natl Acad Sci U S A 102:14069–14074.

Deitch A, Law H, deVere White R. 1982. A stable propidium iodide staining procedure for flow cytometry. J Histochem Cytochem 30:967–972.

Doetsch F, Caille I, Lim DA, Garcia-Verdugo JM, Alvarez-Buylla A. 1999. Subventricular zone astrocytes are neural stem cells in the adult mammalian brain. Cell 97:703–716.

Ito M, Hiramatsu H, Kobayashi K, Suzue K, Kawahata M, Hioki K, Ueyama Y, Koyanagi Y, Sugamura K, Tsuji K, Heike T, Nakahata T. 2002. NOD/SCID/gamma cnull mouse: an excellent recipient mouse model for engraftment of human cells. Blood 100:3175–3182.

Iwanami A, Kaneko S, Nakamura M, Kanemura Y, Mori H, Kobayashi S, Yamasaki M, Momoshima S, Ishii H, Ando K, Tanioka Y, Tamaoki N, Nomura T, Toyama Y, Okano H. 2005. Transplantation of human neural stem cells for spinal cord injury in primates. J Neurosci Res 80:182–190.

Jeong S, Chu K, Jung K, Kim SU, Kim M, Roh J-K. 2003. Human neural stem cell transplantation promotes functional recovery in rats with experimental intracerebral hemorrhage. Stroke 34:2258–2263.

Kanemura Y, Mori H, Kobayashi S, Islam O, Kodama E, Yamamoto A, Nakanishi Y, Arita N, Yamasaki M, Okano H, Hara M, Miyake J. 2002. Evaluation of in vitro proliferative activity of human fetal neural stem/progenitor cells using indirect measurements of viable cells based on cellular metabolic activity. J Neurosci Res 69:869–879.

Keyoung HM, Roy NS, Benraiss A, Louissaint A, Suzuki A, Hashimoto M, Rashbaum WK, Okano H, Goldman SA. 2001. High-yield selection and extraction of two promoter-defined phenotypes of neural stem cells from the fetal human brain. Nat Biotechnol 19:843–850.

Masuda H, Maruyama T, Hiratsu E, Yamane J, Iwanami A, Nagashima T, Ono M, Miyoshi H, Okano HJ, Ito M, Tamaoki N, Nomura T, Okano H, Matsuzaki Y, Yoshimura Y. 2007. Noninvasive and real-time assessment of reconstructed functional human endometrium in NOD/SCID/γ-formula immunodeficient mice. Proc Natl Acad Sci U S A 104:1925–1930.

McBride JL, Behrstock SP, Chen E, Jakel RJ, Irwin Siegel CNS, Kordower JH. 2004. Human neural stem cell transplants improve motor function in a rat model of Huntington's disease. J Comp Neurol 475:211–219.

Miyoshi H, Blomer U, Takahashi M, Gage FH. 1998. Development of a self-inactivating lentivirus vector. J Virol 72:8150–8157.

Murayama A, Matsuzaki Y, Kawaguchi A, Shimazaki T, Okano H. 2002. Flow cytometric analysis of neural stem cells in the developing and adult mouse brain. J Neurosci Res 69:837–847.

Nakamura Y, Yamamoto M, Oda E, Yamamoto A, Kanemura Y, Hara M, Suzuki A, Yamasaki M, Okano H. 2003. Expression of tubulin beta II in neural stem/progenitor cells and radial fibers during human fetal brain development. Lab Invest 83:479–489.

Nicoullon V, Belvindrah R, Rougon G, Chazal G. 2005. mCD24 regulates proliferation of neuronal committed precursors in the subventricular zone. Mol Cell Neurosci 28:462–474.

Okada S, Ishii K, Yamane J, Iwanami A, Ikegami T, Katoh H, Iwamoto Y, Nakamura M, Miyoshi H, Okano HJ, Contag CH, Toyama Y, Okano H. 2005. In vivo imaging of engrafted neural stem cells: its application in evaluating the optimal timing of transplantation for spinal cord injury. FASEB J 19:1839–1841.

Okano H. 2002. Stem cell biology of the central nervous system. J Neurosci Res 69:698–707.

Panchision DM, Chen H-L, Pistollato F, Papini D, Ni H-T, Hawley TS. 2007. Optimized flow cytometric analysis of central nervous system tissue reveals novel functional relationships among cells expressing CD133, CD15, and CD24. Stem Cells 25:1560–1570.

Petty RD, Sutherland LA, Hunter EM, Cree IA. 1995. Comparison of MTT and ATP-based assays for the measurement of viable cell number. J Biolumin Chemilumin 10:29–34.

Piao J, Odeberg J, Samuelsson EB, Kjaeldgaard A, Falci S, Seiger A, Sundstrom E, Akesson E. 2006. Cellular composition of long-term human spinal cord- and forebrain-derived neurosphere cultures. J Neurosci Res 84:471–482.

Pruszak J, Sonntag KC, Aung MH, Sanchez-Pernaute R, Isacson O. 2007. Markers and methods for cell sorting of human embryonic stem cell-derived neural cell populations. Stem Cells 25:2257–2268.

Reynolds B, Weiss S. 1992. Generation of neurons and astrocytes from isolated cells of the adult mammalian central nervous system. Science 255:1707–1710.

Shewan D, Calaora V, Nielsen P, Cohen J, Rougon G, Moreau H. 1996. mCD24, a glycoprotein transiently expressed by neurons, is an inhibitor of neurite outgrowth. J Neurosci 16:2624–2634.

Shultz L, Schweitzer P, Christianson S, Gott B, Schweitzer I, Tennent B, McKenna S, Mobraaten L, Rajan T, Greiner D. 1995. Multiple defects in innate and adaptive immunologic function in NOD/LtSz-scid mice. J Immunol 154:180–191.

Svendsen CN, ter Borg MG, Armstrong RJE, Rosser AE, Chandran S, Ostenfeld T, Caldwell MA. 1998. A new method for the rapid and long term growth of human neural precursor cells. J Neurosci Methods 85:141–152.

Uchida N, Buck DW, He D, Reitsma MJ, Masek M, Phan TV, Tsukamoto AS, Gage FH, Weissman IL. 2000. Direct isolation of human central nervous system stem cells. Proc Natl Acad Sci U S A 97:14720–14725.

Vescovi AL, Parati EA, Gritti A, Poulin P, Ferrario M, Wanke E, Frolichsthal-Schoeller P, Cova L, Arcellana-Panlilio M, Colombo A, Galli R. 1999. Isolation and cloning of multipotential stem cells from the embryonic human CNS and establishment of transplantable human neural stem cell lines by epigenetic stimulation. Exp Neurol 156:71–83.

Wright LS, Prowse KR, Wallace K, Linskens MHK, Svendsen CN. 2006. Human progenitor cells isolated from the developing cortex undergo decreased neurogenesis and eventual senescence following expansion in vitro. Exp Cell Res 312:2107–2120.

Neuroscience Research 65 (2009) 384–392

Contents lists available at ScienceDirect

Neuroscience Research

journal homepage: www.elsevier.com/locate/neures

Transplantation of dendritic cells promotes functional recovery from spinal cord injury in common marmoset

Masae Yaguchi[a], Masanao Tabuse[b], Shigeki Ohta[a], Kozo Ohkusu-Tsukada[a], Tamaki Takeuchi[a], Junichi Yamane[c], Hiroyuki Katoh[c], Masaya Nakamura[c], Yumi Matsuzaki[d], Masayuki Yamada[e,f], Toshio Itoh[f], Tatsuji Nomura[f], Yoshiaki Toyama[c], Hideyuki Okano[d], Masahiro Toda[a,b,*]

[a] Neuroimmunology Research Group, Keio University School of Medicine, Tokyo, Japan
[b] Department of Neurosurgery, Keio University School of Medicine, Tokyo, Japan
[c] Department of Orthopaedic Surgery, Keio University School of Medicine, Tokyo, Japan
[d] Department of Physiology, Keio University School of Medicine, Tokyo, Japan
[e] Faculty of Radiological Technology, Fujita Health University, School of Health Sciences, Aichi, Japan
[f] Central Institute for Experimental Animals, Kawasaki, Kanagawa, Japan

ARTICLE INFO

Article history:
Received 12 February 2009
Received in revised form 21 August 2009
Accepted 31 August 2009
Available online 6 September 2009

Keywords:
Dendritic cells
Spinal cord injury
Non-human primate
Transplantation

ABSTRACT

We previously reported that implantation of dendritic cells (DCs) into the injured site activates neural stem/progenitor cells (NSPCs) and promotes functional recovery after spinal cord injury (SCI) in mice. Working toward clinical application of DC therapy for SCI, we analyzed whether DCs promote functional recovery after SCI in a non-human primate, the common marmoset (CM). CMs are usually born as dizygotic twins. They are thus natural bone marrow and peripheral blood chimeras due to sharing of the placental circulation between dizygotic twins, leading to functional immune tolerance. In this study, to identify adequate CM donor-and-host pairs, mixed leukocyte reaction (MLR) assays were performed. Then, CM-DCs were generated from the bone marrow of the twin selected to be donor and transplanted into the injured site of the spinal cord of the other twin selected to be host, 7 days after injury. Histological analyses revealed fewer areas of demyelination around the injured site in DC-treated CMs than in controls. Immunohistochemical analysis showed that more motor neurons and corticospinal tracts were preserved after SCI in DC-treated CMs. Motor functions were evaluated using three different behavior tests and earlier functional recovery was observed in DC-treated CMs. These results suggest DC therapy to possibly be beneficial in primates with SCI and that this treatment has potential for clinical application.

1. Introduction

Because repair is very limited after central nervous system (CNS) injury, especially in spinal cord injury (SCI), the development of new therapies is urgently needed for CNS injury. Recently, various cell therapies have been studied for the treatment of SCI using ES cells (McDonald et al., 1999), neural stem cells (Cummings et al., 2005; Ogawa et al., 2002, Okano, 2002), bone marrow cells (Koda et al., 2005; Koshizuka et al., 2004), Schwann cells (Martin et al., 1996; Takami et al., 2002), and olfactory ensheathing cells (Doucette, 1995; Richter and Roskams, 2008) in animal models. Immune-cell-based therapy using T cells and macrophages has also been reported for the treatment of SCI (Hauben et al., 2000). Most interestingly, activated macrophages showed a beneficial effect in a human clinical study (Knoller et al., 2005).

Dendritic cells (DCs), which are antigen presentation cells (APCs), have the ability to prime T cells for immune responses against viruses, bacteria and tumors. Immature DCs can capture and process exogenous antigens, and following maturation, migrate to lymphoid organs, where they stimulate potent antigen-specific T cells (Steinman, 1991; Steinman et al., 2003). Based on their strong ability to activate cytotoxic T lymphocytes, DCs are regarded as a useful tool for cancer immunotherapy and are currently being used in human clinical studies for the treatment of various cancers (Banchereau and Palucka, 2005; Nencioni and Brossart, 2004; Schuler et al., 2003). Recently, we reported that implantation of DCs into the injured site of the mouse spinal cord produced functional recovery with *de-novo* neurogenesis (Mikami et al., 2004). Murine DCs were shown to secrete NT-3 and activate neural stem/progenitor cells (NSPCs).

* Corresponding author at: Department of Neurosurgery, Keio University School of Medicine, 35 Shinanomachi, Shinjuku-ku, Tokyo 160-8582, Japan. Tel.: +81 3 5363 3587.
E-mail address: todam@sc.itc.keio.ac.jp (M. Toda).

0168-0102/$ – see front matter © 2009 Elsevier Ireland Ltd and the Japan Neuroscience Society. All rights reserved.
doi:10.1016/j.neures.2009.08.016

Working toward the clinical application of novel therapies, studies using non-human primates are valuable for ensuring both the therapeutic effects and safety (Courtine et al., 2007). Compared with other monkeys, the common marmoset (*Callithrix jacchus*; CM) offers many advantages for preclinical studies (Abbott et al., 2003; Ludlage and Mansfield, 2003; Mansfield, 2003). The average weight of an adult CM is 200–300 g, and adult body length (without tail) is 14–19 cm, making it possible to handle and breed these animals easily on a large scale and thereby reduce the cost of experiments (Ludlage and Mansfield, 2003). CMs have been used in studies on CNS diseases including Parkinson's disease (Gnanalingham et al., 1993), stroke (Marshall et al., 2000), Huntington's disease (Kendall et al., 1998), multiple sclerosis (t Hart et al., 1998, 2004), anxiety (Barros et al., 2000) and SCI (Fouad et al., 2004; Iwanami et al., 2005b; Liu et al., 2001). We recently established culture methods for DCs in CMs (Ohta et al., 2008). With the goal of clinical application of DC therapy, in this study, we analyzed the effects, safety, and feasibility of this therapy in a SCI model of CM.

2. Materials and methods

2.1. Animals and spinal cord injury

Adult CM (260–400 g; 1–2 years old, Clea Japan Inc., Tokyo, Japan) were used in this study. Contusive SCIs were induced using a weight-drop device (a modified NYU impactor with a diameter of 3.5 mm) as described previously (Iwanami et al., 2005a). After an intramuscular injection of ketamine (50 mg/kg) and xylazine (5 mg/kg) to induce anesthesia, a C5 laminectomy was carried out and a 17 g weight was dropped from a height of 50 mm onto the exposed dura matter (Iwanami et al., 2005a). A week after injury, $4–8 \times 10^6$ DCs in 10–15 μl of RPMI medium (Sigma, St. Louis, MO) or RPMI-1640 medium (10–15 μl) were injected into the center of the lesion site using a micro-stereotaxic injection system (David Kopf Instruments, Tujunga, CA). All animals received daily ampicillin (100 mg/kg intramuscularly; Meiji Seika Kaisha, Ltd., Tokyo, Japan) for 1 week after injury. The ethics committee of the institute approved all surgical interventions and animal care procedures, which were carried out in accordance with the Laboratory Animal Welfare Act, the Guide for the Care and Use of Laboratory Animals (National Institutes of Health, USA), and the Guidelines and Policies for Animal Surgery provided by the Animal Study Committees of the Central Institute for Experimental Animals and Keio University.

2.2. Mixed leukocyte reactions (MLR)

The peripheral blood mononuclear cells (PBMCs) in CM were prepared using Lymphoprep (Fresenius Kabi Norge, Halden, Norway). Then, PBMCs were divided into stimulators and responders. The stimulators irradiated at 40 Gy were co-cultured with responders (each 1×10^5 cells) in triplicate in 96 U-well plates (Costar Corp.) for 6 days. PHA (phytohaemagglutinin, Sigma, 2 μg/mL), autologous PBMCs, and allogeneic PBMCs were used as controls in each experiment. The cultures were pulsed with 18.5 kBq/well [^{3}H]-thymidine (Amersham) for 8 h on day 6, and then harvested onto fiber-coated 96-well plates (Packard Instruments, Groningen, Netherlands). Radioactivity was measured using a Top count (Packard Instruments).

2.3. Cell culture and flowcytometric analysis

DCs were generated from bone marrow (BM) cells as previously described (Ohta et al., 2008). Femurs and tibiae of CM were removed and left in 70% ethanol for a few minutes before washing in phosphate buffered saline (PBS). Both ends were cut with scissors and BM cells were cultured in RPMI-1640 supplemented with 10% heat-inactivated fetal calf serum (FCS). After overnight incubation, suspended cells were collected and further cultured in a complete medium (cRPMI), which consisted of RPMI-1640 supplemented with 10% FCS, penicillin and streptomycin (50 U/mL, Invitrogen, Carlsbad, CA), recombinant human (rh) GM-CSF (100 ng/mL; Leukine, Berlex Laboratories, Richmond, CA), and rhIL-4 (100 ng/mL; PeproTech Inc, Rocky Hills, NY). Half the supernatant was replenished with fresh cRPMI on culture day 4, and the floating cells were collected as a DC-enriched cell fraction on culture day 7. On day 7 of culture, cells were stained with anti-human CD11c (clone S-HCL-3, Becton Dickinson, San Jose, CA) and anti-human HLA-DR (clone G46-6, BD Pharmingen, San Diego, CA) antibodies, and then double positive cells were sorted using FACS vantage (BD Biosciences, San Jose, CA) and Moflo (Dako Cytometry, Kyoto, Japan).

2.4. Electron microscopy analysis

Cells were fixed with 2.5% glutaraldehyde and 4% paraformaldehyde (PFA) in 0.1 M cacodylate buffer (pH 7.4) and post-fixed with 1% OsO_4. After dehydration in a graded ethanol series, the cells were embedded in Epon (Oukenshoji, Tokyo). After preparation of semithin sections (0.1 μm), images were obtained using an electron microscope (Japanese Electronic Optical Laboratories, JEOL-1230).

2.5. Magnetic resonance imaging (MRI)

The magnitude of the SCI was monitored by examining changes in intramedullary magnetic resonance imaging (MRI) signals (Metz et al., 2000). MR imaging were performed by using a 7.0 T MR imager (PharmaScan 70/16; Bruker Biospin, Ettlingen, Germany) equipped with the integrated transmitting and receiving coil (i.d. 62 mm) under following conditions: sagittal, coronal, axial T2-weighted fast spin-echo, and sagittal T1-weighted spin-echo.

2.6. Histological analyses

Eight weeks after DC-transplantation, the CM models were perfused with 4% PFA. The dissected spinal cord tissues were post-fixed overnight in 4% PFA, then soaked overnight in 10% followed by 30% sucrose. Serial axial sections (12 μm thickness) were collected every 600 μm over a length of 7200 μm (rostral 1200 μm and caudal 6000 μm to the epicenter). For hematoxylin–eosin (HE) staining, sagittal sections containing the epicenter were also prepared. Some sections were stained with anti-choline acetyltransferase (ChAT) antibody (Ab) (1:200, mouse IgG; Chemicon International, Inc., Temecula, CA), followed by a horseradish peroxidase [HRP]-labeled anti-mouse IgG (1:400, goat IgG; Jackson Laboratory, Bar Harbor, ME). The ABC method was used to detect labeled cells using a Vectastain kit (Vector Laboratories, Burlingame, CA). Sections were also stained with anti-calmodulin-dependent protein kinase IIα (CaMK-IIα) Ab (1:50, mouse monoclonal; Zymed, CA), to detect the corticospinal tract (CST), followed by a secondary antibody, Alexa Fluor 568-conjugated anti-mouse IgG (1:400, goat IgG; Invitrogen).

The myelinated area was analyzed by staining with Luxol fast blue (LFB, Sigma). Images were obtained using Zeiss AxioCam 4.4 (Zeiss) and were converted into binary images using NIH Image software. In the converted binary images, areas with a higher staining intensity than the threshold of LFB staining were defined as myelinated areas. The threshold values were maintained at a constant level for all the analyses. Motor neurons in the ventral horn were analyzed using ChAT staining, and the corticospinal tract area was analyzed using CaMK-IIα staining. Images were

obtained using Zeiss AxioCam 4.4, and these images were analyzed using NIH Image software.

2.7. Behavioral analyses

The behavioral tests were examined according to the previous reports (Iwanami et al., 2005b). They can be summarized as follows.

2.7.1. Bar grip test

The motor function of the upper extremities was evaluated by the bar grip test using device (220 mm wide, 500 mm deep, and 400 mm high with a bar diameter of 2.5 mm in a 1 × 3 [70 mm × 100 mm] grid pattern), which analyzes the animal's gripping reflex (the motion undertaken when attempting to grasp an object placed before the animal). The percentage of the maximal grip strength relative to that before the injury was calculated for each day after the injury.

2.7.2. The behavioral scoring test

Each CM was observed for 5 min to assess its ability to perform the basic motions, scored as follows (Iwanami et al., 2005b): score 1, changing from a supine to a prone position; score 2, grasping the cage with its forelimbs; score 3, rasping the cage with its hindlimbs; score 4, walking, with weight bearing, on its forelimbs; score 5, walking, with weight bearing on its hindlimbs; score 6, a single jump; score 7, multiple jumps; score 8, sitting or standing for more than 3 s; and score 9, smooth movements without falling through the gaps between the cage bars. Each animal's score was determined by two independent observers. With scores ranging from 1 to 9, one score was given for each representative motion that was accomplished successfully.

The bargrip test and the behavioral scoring test were performed in a double-blinded manner.

2.7.3. Measurements of spontaneous motor activity

Cages (350 mm wide, 500 mm deep, and 500 mm high) were equipped with infrared sensors (Murata Manufacturing Corp., Nagaokakyo, Kyoto, Japan) on the ceiling to continually record the 3D motion of CMs. This system utilizes a passive thermographic infrared sensor to monitor the heat emitted from the animals. The 3D localization of the heat source was monitored, and a change in this localization was recorded as movement. Each animal's data were recorded and monitored on a computer on an hourly basis, and the activity count after SCI was calculated as a percentage relative to that before the injury.

2.8. Statistical analysis

Student's *t*-test was used to analyze statistically significant differences in immunohistochemical results. The Mann–Whitney *U*-test was used to analyze statistically significant differences in behavioral test results. Data are presented as the mean ± standard error of the mean (SEM) with $^{*}P < 0.05$, $^{**}P < 0.01$, and $^{***}P < 0.001$.

3. Results

3.1. Identification of donor-and-host pairs for DC-transplantation

In this study, DCs were generated from the BM of a CM twin and the generated DCs were transplanted into the other CM twin. To exclude the possibility of allograft rejection between dizygotic twins, an MLR assay was performed. The MLR assay results for the 27 pairs of CM twins are shown in Table 1. Twenty-one of the 27 pairs of CM twins were MLR negative and were used as donor–host pairs for transplantation. In contrast, 6 pairs of the CM twins were

Table 1
Results of the mixed leukocyte reactions (MLR) assay for the screening of donor–host pair.

Twins	PHA	Auto	Allo	Check	Twins	PHA	Auto	Allo	Check	Twins	PHA	Auto	Allo	Check
A1	1606 ± 661	100 ± 11	247 ± 43	99 ± 26	L1	2626 ± 1529	100 ± 7	151 ± 10	127 ± 14	a1	1050 ± 327	100 ± 47	175 ± 54	188 ± 46
A2	1407 ± 1023	100 ± 31	331 ± 52	133 ± 4	L2	6738 ± 966	100 ± 10	149 ± 22	116 ± 18	a2	1848 ± 903	100 ± 36	277 ± 102	122 ± 25
B1	2129 ± 387	100 ± 54	143 ± 45	78 ± 15	M1	446 ± 55	100 ± 9	162 ± 29	96 ± 12	b1	553 ± 101	100 ± 9	110 ± 8	116 ± 9
B2	2194 ± 227	100 ± 14	377 ± 45	84 ± 16	M2	1407 ± 1023	100 ± 31	331 ± 52	133 ± 4	b2	16682 ± 3312	100 ± 39	159 ± 32	131 ± 16
C1	663 ± 385	100 ± 18	814 ± 138	121 ± 6	N1	2935 ± 1709	100 ± 18	109 ± 14	96 ± 15	c1	3813 ± 810	100 ± 22	170 ± 57	394 ± 204
C2	782 ± 112	100 ± 41	143 ± 85	107 ± 14	N2	6464 ± 926	100 ± 12	150 ± 21	121 ± 23	c2	661 ± 278	100 ± 41	202 ± 60	413 ± 109
D1	7898 ± 1625	100 ± 8	197 ± 65	100 ± 16	O1	7607 ± 3201	100 ± 8	673 ± 111	68 ± 4	d1	4505 ± 822	100 ± 21	139 ± 14	123 ± 10
D2	2795 ± 520	100 ± 16	144 ± 14	83 ± 8	O2	9234 ± 3652	100 ± 25	206 ± 12	291 ± 84	d2	60202 ± 1195	100 ± 11	121 ± 13	149 ± 16
E1	7130 ± 1623	100 ± 16	86 ± 14	100 ± 17	P1	4176 ± 1507	100 ± 6	225 ± 14	127 ± 3	e1	7295 ± 2274	100 ± 10	128 ± 3	121 ± 19
E2	18613 ± 232	100 ± 24	280 ± 11	148 ± 63	P2	1373 ± 290	100 ± 19	212 ± 21	103 ± 44	e2	4590 ± 1599	100 ± 11	113 ± 6	122 ± 34
F1	15409 ± 1967	100 ± 12	163 ± 44	113 ± 22	Q1	1848 ± 903	100 ± 36	277 ± 102	122 ± 25	f1	3491 ± 2033	100 ± 19	243 ± 16	224 ± 74
F2	17692 ± 2033	100 ± 13	190 ± 35	104 ± 17	Q2	4785 ± 437	100 ± 14	347 ± 134	90 ± 11	f2	3740 ± 536	100 ± 20	168 ± 33	260 ± 118
G1	4651 ± 1399	100 ± 31	470 ± 305	125 ± 30	R1	30370 ± 6250	100 ± 17	179 ± 19	100 ± 8					
G2	678 ± 43	100 ± 10	158 ± 37	90 ± 43	R2	17962 ± 3345	100 ± 8	131 ± 20	119 ± 19					
H1	5219 ± 805	100 ± 10	635 ± 71	141 ± 6	S1	42365 ± 9643	100 ± 7	156 ± 9	111 ± 19					
H2	1380 ± 810	100 ± 24	200 ± 39	162 ± 28	S2	6555 ± 1606	100 ± 40	151 ± 12	108 ± 29					
I1	953 ± 207	100 ± 28	145 ± 6	90 ± 24	T1	2742 ± 487	100 ± 15	161 ± 24	131 ± 14					
I2	8735 ± 810	100 ± 32	444 ± 207	107 ± 26	T2	41893 ± 8601	100 ± 14	152 ± 14	106 ± 14					
J1	398 ± 70	100 ± 45	301 ± 174	145 ± 27	U1	14329 ± 2610	100 ± 24	159 ± 37	140 ± 30					
J2	1537 ± 399	100 ± 13	127 ± 66	129 ± 54	U2	1220 ± 727	100 ± 13	145 ± 13	83 ± 15					
K1	2710 ± 52	100 ± 12	296 ± 38	100 ± 18										
K2	760 ± 75	100 ± 16	224 ± 31	105 ± 10										

The value of autologous reaction is referred to 100. Each value indicates the percentage of radioactivity relative to that of autologous reaction (mean ± SD). Twenty-one pairs of twins (A–U) are MLR negative and 6 pairs of twins (a–f) are MLR positive.

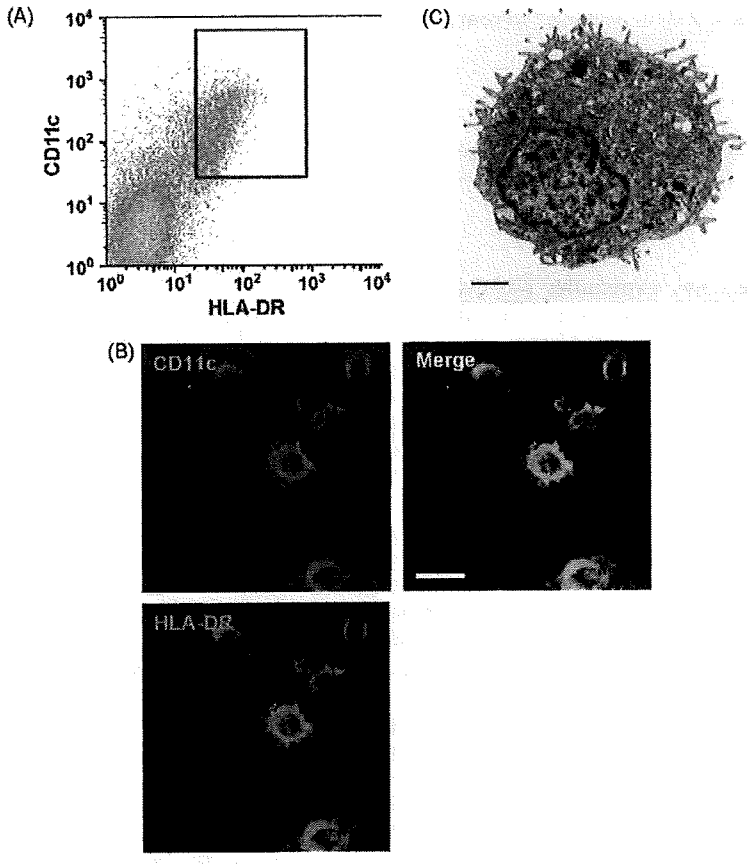

Fig. 1. Purification and characterization of common marmoset dendritic cells (CM-DCs). (A) Flow cytometric analysis of cultured bone marrow (BM) in the presence of rhGM-CSF and rhIL-4 for a week. $CD11c^{+}HLA\text{-}DR^{+}$ cells (boxed area) were isolated as CM-DCs. (B) Typical images of CM-DCs stained for CD11c (red) and HLA-DR (green) antibodies. Scale bar, 20 μm. (C) Electron microscopic analysis of CM-DCs. Scale bar, 1 μm. (For interpretation of the references to color in this figure legend, the reader is referred to the web version of the article.)

MLR positive and thus were not used for further DC-transplantation experiments.

3.2. Purification and characterization of DCs from bone marrow

DCs were cultured for a week in the presence of hrGM-CSF and hrIL-4 from the BM of CM as described previously (Ohta et al., 2008). CM-DCs were purified as cells double-labeled for CD11c and HLA-DR antibodies using flow cytometry (Fig. 1A). Approximately 4–8 × 10^6 DCs were purified from 1 to 5 × 10^8 BM cells of a CM. A typical image of BM-derived DCs stained with CD11c and HLA-DR antibodies is shown in Fig. 1B. Electron microscopic analysis of CM-DCs showed an eccentric nucleus and the presence of small dendrites consistent with typical DC morphology (Fig. 1C).

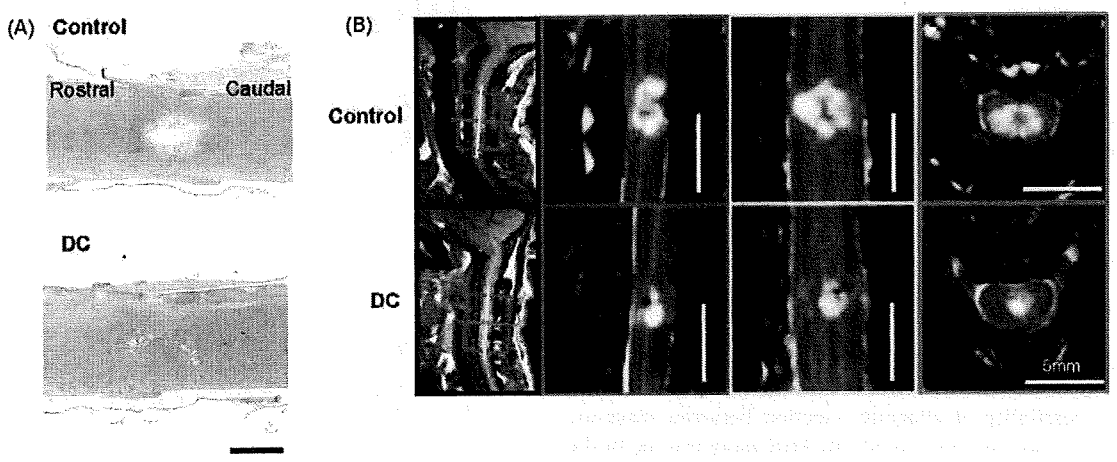

Fig. 2. Histological and magnetic resonance images (MRI) of the injured spinal cord in CMs 8 weeks after DC-transplantation. (A) H&E staining of sagittal sections of injured spinal cords in DC-transplanted CM (animal No. U2 in Table 1) and control. Scale bar, 1 mm. (B) Sagittal, coronal, and axial MR images (T2WI) of injured spinal cords in CMs. The DC-treated CM is animal No. B1. The lesion was visible as a hyperintense signal on T2WI-MRI. Scale bar, 5 mm.

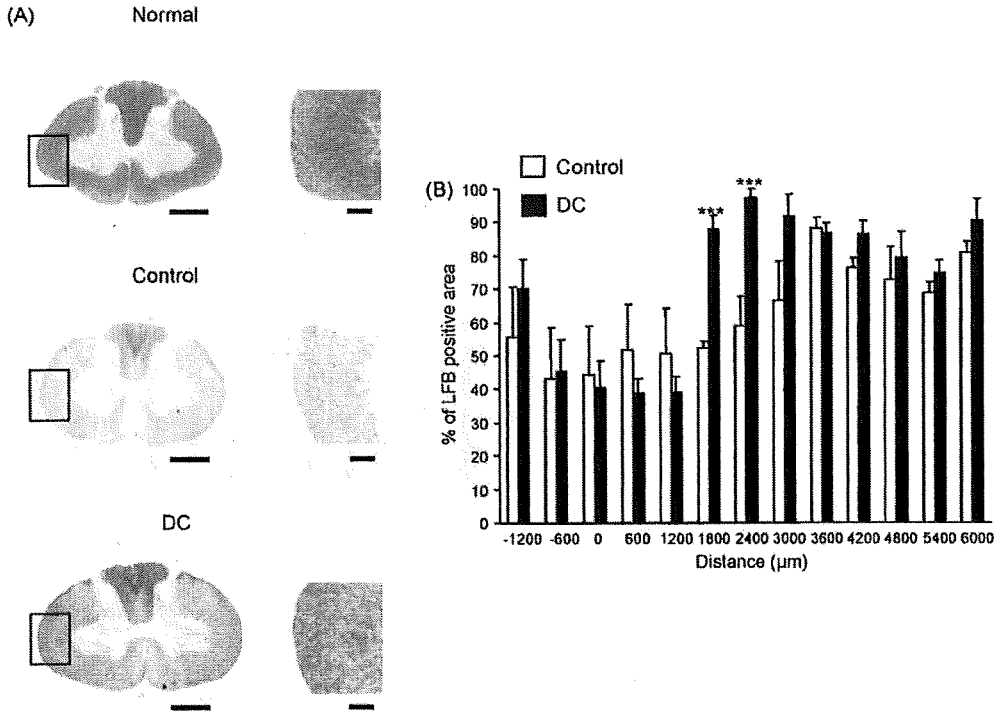

Fig. 3. Quantitative analysis of myelinated areas around the epicenter 8 weeks after transplantation. (A) Representative LFB-stained specimens from normal CM, control CM and DC-treated CM (animal No. 01). Scale bar, 1 mm. Scale bar for enlarged image of boxed area, 250 μm. (B) Cranio-caudal distribution (total length of 7200 μm; 1200 μm rostral (−) and 6000 μm caudal (+) to the epicenter) of the LFB-positive area in control and DC-treated CMs. The percentage of the LFB-positive area relative to the corresponding area in the intact CM was calculated using NIH image software. DCs-treatment, $n = 6$; control, $n = 5$. ***$P < 0.001$.

3.3. Lesion size reduction with DC-transplantation

Seven days after injury, 4–8 × 10^6 DCs generated from the BM of a donor CM twin were transplanted into the injured site of the spinal cord of a host CM twin. Histochemical analysis showed the spinal cord lesion to be smaller in a DC-transplanted CM than in a control 8 weeks after DC-transplantation (Fig. 2A). On MRI, T2-weighted images (T2WI) showed a hyperintense signal in the injured spinal cord of the control CM 8 weeks after injury and the signal in the DC-transplanted CM was smaller than that of control (Fig. 2B).

3.4. Immunohistochemical analyses

Axial sections of spinal cords in either DC- or RPMI-treated CMs 8 weeks after transplantation were subjected to immunological analyses to determine the effects of DC-transplantation. We collected serial axial sections every 12 μm in a total length of 7200 μm (1200 μm rostral and 6000 μm caudal to the epicenter). The LFB staining showed a decrease in demyelinated areas caudal to the epicenter in DC-transplanted CMs as compared to that of controls (Fig. 3). In a monkey, CST fibers project to the ventral horn, and some axons synapse directly on motor neurons innervating hand muscles (Lemon et al., 2004). The number of ChAT-positive motor neurons in the ventral horn was greater in DC-treated CMs than in controls in areas caudal to the lesion site (Fig. 4). We further measured the density of nerve fibers that stained positively for CaMK-IIα (Terashima et al., 1994). CaMK-IIα-positive CST fibers were observed in the lateral funiculus, and immunoreactivity of CaMK-IIα in DC-treated CMs was greater than that in controls in some areas caudal to the lesion site (Fig. 5).

3.5. Behavioral recovery after DC-transplantation

To examine the effect of DC-transplantation, we performed three different behavioral analyses established by Iwanami et al. (2005a); bar grip test, behavior scoring tests, and measurement of spontaneous motor activity. The corticospinal system is involved in dexterous hand movements. To evaluate the recovery of forelimb motor function, bar grip tests were conducted on described days. The bar grip strength sharply decreased in both groups immediately after injury. After transplantation, DC-treated CMs showed significant recovery, with higher bar grip power values than the controls at 1, 3, 7, and 8 weeks after transplantation (Fig. 6A). The behavioral scoring test assesses the recovery of motor function in the forelimbs and hindlimbs (Iwanami et al., 2005b). DC-treated groups showed significant recovery as compared to controls at 1, 4, and 5 weeks after transplantation (Fig. 6B). In the measurement of spontaneous three-dimensional movement using a sensor placed in the cages, the values in both groups decreased sharply after injury. After DC-transplantation, DC-treated animals tended to show earlier recovery than controls, although the difference was not statistically significant (Fig. 6C).

The monitoring of spontaneous 3D movement is an objective behavior analysis; however, such monitoring assesses not only motor function, but also general physical condition. Thus, the general physical condition of the mice might have affected the results. Further behavior analyses will be required to assess the details of motor function in CMs after SCI.

4. Discussion

Our current results demonstrate that transplantation of DCs contributes to the functional recovery of SCI in a non-human

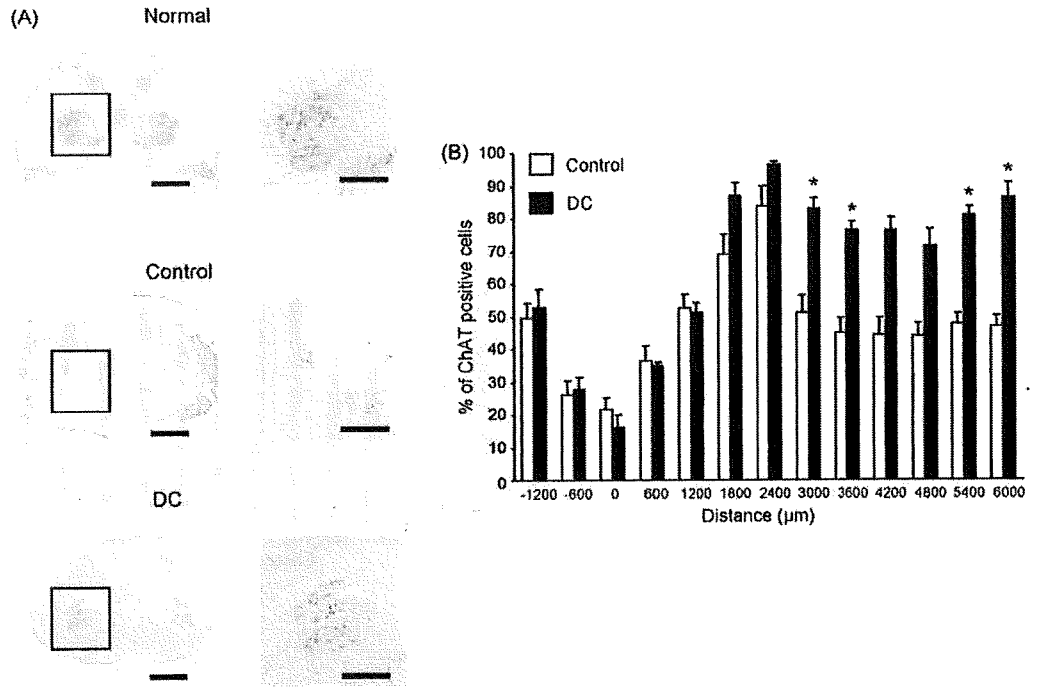

Fig. 4. Quantitative analysis of the number of ChAT-positive neurons in the ventral horn around the epicenter 8 weeks after transplantation. (A) Anti-ChAT immunostaining. ChAT-positive cells are observed in the ventral horn of the spinal cord as shown in the boxed area. The DC-treated CM is animal No. 01. Scale bar, 1 mm. Scale bar for enlarged image of boxed area, 500 μm. (B) Cranio-caudal distribution (total length of 7200 μm; 1200 μm rostral (−) and 6000 μm caudal (+) to the epicenter) of the ChAT-positive area in control and DCs-treated CMs. DC-treatment, $n = 6$; control, $n = 5$. $^*P < 0.05$.

primate SCI model using CM. In our previous study using a mouse SCI model, DC-transplantation enhanced axonal sprouting caudal to the lesion site (Mikami et al., 2004). One of the mechanisms underlying the enhancement of axonal sprouting by DCs is suggested to be increased NT-3 level, within the injured spinal cord, which is secreted from implanted mouse DCs. NT-3 is known to promote axonal growth in the spinal cord (Grill et al., 1997) and support the remyelination in SCI (McTigue et al., 1998; Girard et al., 2005). Recently, we demonstrated that CM-DCs also express NT-3 (Ohta et al., 2008). In this study, immunohistochemical analyses showed a decrease in neuronal loss and demyelination in the areas caudal to the lesion site in response to DC-transplantation. Although further studies are required to analyze descending fibers including CST in the CM-SCI model in detail, NT-3 secreted by DCs may exert a neuroprotective effect by decreasing neuronal loss and axonal damage.

We previously demonstrated the *de-novo* neurogenesis accompanied by the increase in NSPCs after DC-transplantation in a mouse SCI model (Mikami et al., 2004). In this study, we could not analyze either neurogenesis or NSPCs in the injured CM spinal cord due to technical difficulties. However, in our preliminary study, CM-DCs increased the number of human NSPCs *in vitro* (unpublished data). Thus, CM-DCs might have increased the number of neurons in the spinal cord via *de-novo* neurogenesis accompanied by the activation of endogenous NSPCs. It is also possible that activation of endogenous NSPCs might increase oligodendrocyte

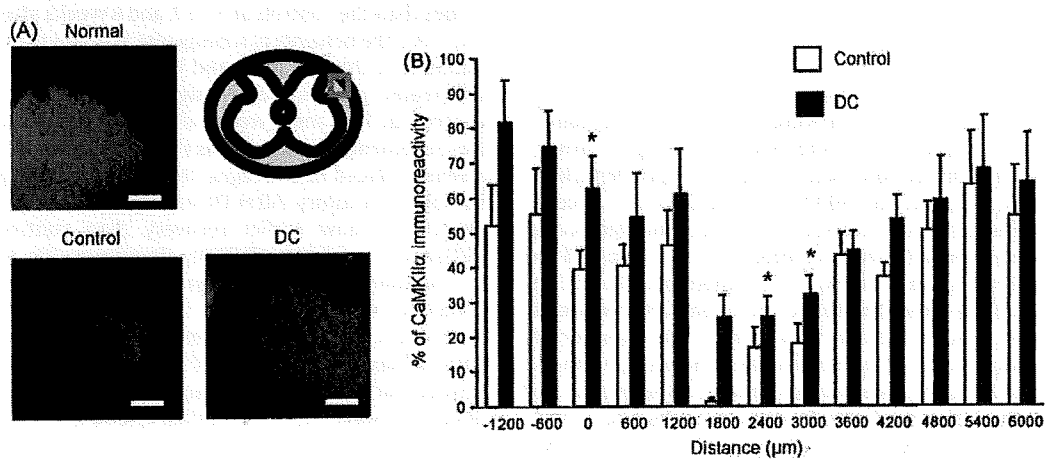

Fig. 5. Quantitative analysis of CaMK-IIα positive area around the epicenter 8 weeks after transplantation. (A) Enlarged images of boxed areas that are stained with CaMK-IIα antibody in the lateral funiculus are shown. The DC-treated CM is animal No. 01. Scale bar, 100 μm. (B) Cranio-caudal distribution (total length of 7200 μm; 1200 μm rostral (−) and 6000 μm caudal (+) to the epicenter) of the CaMK-IIα positive area (boxed area in A) in control and DC-treated CMs. The percentage of the CaMK-IIα positive area relative to the corresponding area in the intact CM was calculated using NIH image software. DCs-treatment, $n = 6$; control, $n = 5$. $^*P < 0.05$.